



---

Year: 2020

---

## **Consensus recommendations for a dynamic susceptibility contrast MRI protocol for use in high-grade gliomas**

Boxerman, Jerrold L ; Quarles, Chad C ; Hu, Leland S ; Erickson, Bradley J ; Gerstner, Elizabeth R ; Smits, Marion ; Kaufmann, Timothy J ; Barboriak, Daniel P ; Huang, Raymond H ; Wick, Wolfgang ; Weller, Michael ; Galanis, Evanthia ; Kalpathy-Cramer, Jayashree ; Shankar, Lalitha ; Jacobs, Paula ; Chung, Caroline ; van den Bent, Martin J ; Chang, Susan ; Al Yung, W K ; Cloughesy, Timothy F ; Wen, Patrick Y ; Gilbert, Mark R ; Rosen, Bruce R ; Ellingson, Benjamin M ; Schmainda, Kathleen M

**Abstract:** Despite the widespread clinical use of dynamic susceptibility contrast (DSC) MRI, DSC-MRI methodology has not been standardized, hindering its utilization for response assessment in multicenter trials. Recently, the DSC-MRI Standardization Subcommittee of the Jumpstarting Brain Tumor Drug Development Coalition issued an updated consensus DSC-MRI protocol compatible with the standardized brain tumor imaging protocol (BTIP) for high-grade gliomas that is increasingly used in the clinical setting and is the default MRI protocol for the National Clinical Trials Network. After reviewing the basis for controversy over DSC-MRI protocols, this paper provides evidence-based best practices for clinical DSC-MRI as determined by the Committee, including pulse sequence (gradient echo vs spin echo), BTIP-compliant contrast agent dosing (preload and bolus), flip angle (FA), echo time (TE), and post-processing leakage correction. In summary, full-dose preload, full-dose bolus dosing using intermediate (60°) FA and field strength-dependent TE (40-50 ms at 1.5 T, 20-35 ms at 3 T) provides overall best accuracy and precision for cerebral blood volume estimates. When single-dose contrast agent usage is desired, no-preload, full-dose bolus dosing using low FA (30°) and field strength-dependent TE provides excellent performance, with reduced contrast agent usage and elimination of potential systematic errors introduced by variations in preload dose and incubation time.

DOI: <https://doi.org/10.1093/neuonc/noaa141>

Posted at the Zurich Open Repository and Archive, University of Zurich

ZORA URL: <https://doi.org/10.5167/uzh-191394>

Journal Article

Accepted Version

Originally published at:

Boxerman, Jerrold L; Quarles, Chad C; Hu, Leland S; Erickson, Bradley J; Gerstner, Elizabeth R; Smits, Marion; Kaufmann, Timothy J; Barboriak, Daniel P; Huang, Raymond H; Wick, Wolfgang; Weller, Michael; Galanis, Evanthia; Kalpathy-Cramer, Jayashree; Shankar, Lalitha; Jacobs, Paula; Chung, Caroline; van den Bent, Martin J; Chang, Susan; Al Yung, W K; Cloughesy, Timothy F; Wen, Patrick Y; Gilbert, Mark R; Rosen, Bruce R; Ellingson, Benjamin M; Schmainda, Kathleen M (2020). Consensus recommendations for a dynamic susceptibility contrast MRI protocol for use in high-grade gliomas. *Neuro-Oncology*, 22(9):1262-1275.

DOI: <https://doi.org/10.1093/neuonc/noaa141>

# Neuro-Oncology

## Consensus Recommendations for a Dynamic Susceptibility Contrast MRI Protocol for Use in High-Grade Gliomas

--Manuscript Draft--

<b>Manuscript Number:</b>	N-O-D-20-00183R1
<b>Full Title:</b>	Consensus Recommendations for a Dynamic Susceptibility Contrast MRI Protocol for Use in High-Grade Gliomas
<b>Short Title:</b>	Revised Protocol Recommendations for DSC-MRI
<b>Article Type:</b>	Review
<b>Keywords:</b>	DSC-MRI; Cerebral Blood Volume; high-grade glioma; clinical trial; consensus protocol
<b>Corresponding Author:</b>	Jerrold Boxerman, MD, PhD Rhode Island Hospital Providence, RI UNITED STATES
<b>Corresponding Author E-Mail:</b>	jerrold.boxerman@gmail.com
<b>Order of Authors:</b>	Jerrold Boxerman, MD, PhD
	Chad C. Quarles
	Leland S. Hu
	Bradley J. Erickson
	Elizabeth R. Gerstner
	Marion Smits
	Timothy J. Kaufmann
	Daniel P. Barboriak
	Raymond H. Huang
	Wolfgang Wick
	Michael Weller
	Evanthia Galanis
	Jayashree Kalpathy-Cramer
	Lalitha Shankar
	Paula Jacobs
	Caroline Chung
	Martin J. van den Bent
	Susan Chang
	W.K. Al Yung
	Timothy F. Cloughesy
	Patrick Y. Wen
	Mark R. Gilbert
	Bruce R. Rosen
	Benjamin M. Ellingson
	Kathleen M. Schmainda
<b>Manuscript Region of Origin:</b>	UNITED STATES

<b>Abstract:</b>	<p>Despite the widespread clinical use of dynamic susceptibility contrast (DSC) MRI, DSC-MRI methodology has not been standardized, hindering its utilization for response assessment in multi-center trials. Recently, the DSC-MRI Standardization Subcommittee of the Jumpstarting Brain Tumor Drug Development Coalition issued an updated consensus DSC-MRI protocol compatible with BTIP, the standardized brain tumor imaging protocol for high-grade gliomas that is increasingly used in the clinical setting and is the default MRI protocol for the National Clinical Trials Network. After reviewing the basis for controversy over DSC-MRI protocols, this manuscript provides evidence-based best practices for clinical DSC-MRI as determined by the Committee, including pulse sequence (gradient echo vs. spin echo), BTIP-compliant contrast agent dosing (preload and bolus), flip angle (FA), echo time (TE), and post-processing leakage correction. In summary, full-dose preload, full-dose bolus dosing using intermediate (60°) FA and field strength-dependent TE (40-50ms at 1.5T, 20-35ms at 3T) provides overall best accuracy and precision for cerebral blood volume estimates. When single-dose contrast agent usage is desired, no-preload, full-dose bolus dosing using low FA (30°) and field strength-dependent TE provides excellent performance, with reduced contrast agent usage and elimination of potential systematic errors introduced by variations in preload dose and incubation time.</p>
<b>Additional Information:</b>	
<b>Question</b>	<b>Response</b>
<p>Are you willing to pay for the publication of color figures in your main manuscript (not supplement)? The price for full color reproduction is approximately £350/\$600/525 EUR per figure. If you submit color figures with your paper then you will be expected to pay if it is accepted.</p>	<p>No, I have no color figures.</p>



BROWN  
Alpert Medical School

JERROLD L. BOXERMAN, M.D., PH.D., F.A.C.R.  
Professor of Diagnostic Imaging  
Director of Diagnostic Neuroradiology  
Rhode Island Hospital and  
Alpert Medical School of Brown University

May 24, 2020

Neuro-Oncology Editorial Office

Dear Editor:

On behalf of my co-authors, I wish to thank you and the reviewers for the conditional acceptance of manuscript N-O-D-20-00183. We found the reviewer's comments and suggestions to be substantive and constructive and are thankful to have been given the opportunity to strengthen our manuscript. I am resubmitting our revised manuscript N-O-D-20-00183R1, which is again entitled: "*Consensus Recommendations for a Dynamic Susceptibility Contrast MRI Protocol for Use in High-Grade Gliomas.*" There have been no changes to the title or author list. Please note that no figures or tables are copied directly from another source.

Our point-by-point response to each reviewer's comments can be found in the uploaded *Response to Reviewer's Comments* document. Common themes to the reviewer's comments included inquiry about more specific recommendations for post-processing of the DSC-MRI data, including leakage correction. We feel that we addressed these questions and comments to the best of our ability and hope that you and the reviewers find our responses to be satisfactory.

I wish to again thank you for consideration of our manuscript. Please do not hesitate to contact me with any questions or concerns regarding our re-submission.

Sincerely,

A handwritten signature in black ink, appearing to read 'Jerrold L. Boxerman'.

Jerrold L. Boxerman, M.D., Ph.D., F.A.C.R.

## Response to reviewer's comments

### Reviewer 1

These consensus recommendations are a great step forwards in brain tumor imaging, since results between different institutions remain incomparable until a standardization is lacking.

There is only one point to consider in the paragraph "Variability of DSC-MRI Methodology in the Literature". Authors discuss the heterogeneity of the results, with a special attention on the threshold values of rCBV to assess treatment response. There is always a residual clinical uncertainty, since even the gold standard of histopathological diagnosis has its weaknesses and most studies are based mainly on clinical course parameters.

*The reviewer raises an excellent point: gold standards for histology and clinical outcomes are difficult to come by. We included this section in the manuscript to provide an example of how literature results regarding the use of CBV for distinguishing true progression from pseudoprogression can appear to lack consistency. It is true that the methodologies and gold standards used for the establishment of these thresholds differ from site to site, but the point is that differences in acquisition protocol are suspected to greatly impact clinical interpretation, thereby motivating our establishment of a consensus DSC-MRI protocol. The DRO work by Quarles et al that we cite in the same section of our manuscript emphasizes this point, since the DRO-based simulations eliminate issues regarding gold standard histopathological diagnosis and isolate the ambiguity in threshold determination due to heterogeneity of acquisition and post-processing methodology.*

Authors should consider another very important issue before officially making recommendations: The critical ROI selection. Most of the DSC perfusion studies found that the use of maximum rCBV instead of the mean has fundamental impact on diagnostic value of the method. The best measure to establish diagnostic threshold values is the relative rCBV value, related to the anatomically mirrored normal appearing tissue region of the contralateral hemisphere. In addition, it should be avoided to integrate vessels in the measuring ROI. For this purpose, post-processing tools providing a co-registered underlay of the contrast-enhanced T1-w image is crucial to measure the rCBV. Strictly speaking, these points are not part of the sequence parameters (MR protocol), but they are a very important part of post-processing and thus for the diagnostic accuracy.

*We thank the reviewer for raising these excellent points. ROI selection is critical, and clinical results will indeed differ depending on whether mean or maximum CBV is used, and whether relative or standardized CBV maps are interpreted. However, the primary focus of this manuscript is the DSC-MRI acquisition protocol (i.e., particulars of the DSC-MRI CBV map generation process), including contrast agent dosing, MRI acquisition parameters, and post-processing of the DSC-MRI signal. We have therefore purposefully avoided*

*discussion of CBV analysis tools and methodologies. These are very important issues and would merit their own consensus recommendations. We believe that a crucial first step for the universal applicability of DSC-MRI is unification of the acquisition protocol, which we hope to have achieved with this manuscript. In theory, if DSC-MRI data are collected in a standardized way in multi-center clinical trials, then we can compare multiple post-processing and lesion selection methodologies in the future.*

*It may very well be the case that it will take acceptance of a single CBV analysis software implementation by the neuro-oncology community for widespread use with reproducible results to be achieved, similar to the acceptance of IschemaView RAPID software for thrombectomy trials by the interventional neuroradiology community. This is suggested by results from Bell et al. (Tomography. 2019 Mar;5(1):110-117; Ref. [63] in our manuscript) that demonstrated marked inter-site disagreement in computed rCBV when site-specific software from 12 sites was applied to a common set of DSC-MRI source data. Issues related to CBV map generation and analysis are complex and are being actively explored and will require a separate consensus paper.*

## **Reviewer 2**

Excellent review of theory and literature to justify consensus DSC MRI recommendations. Minor suggestions below:

Page 9- do the authors mean "regimes" or "regimens" ?

*The reviewer raises an excellent question, since “regime” is often confused with “regimen.” In this case, we do believe that “regime” is appropriate. According to Google Dictionary, definitions include “the conditions under which a scientific or industrial process occurs,” and we are using “limited regimes” to describe the few sets of physiological and experimental conditions for which the MR signal loss due to susceptibility contrast can be described analytically.*

Page 11- perhaps request permission to reprint Fig 5 of Ref. [42]

*We thank the reviewer for this suggestion. We made a very strong effort to abide by the limitation of 7 total figures and tables for review articles in this Journal. We believe that the figures and tables that we have selected are integral to the manuscript. In fact, we have already relegated the tables summarizing the consensus protocol to supplementary material. Although in principle Fig. 5 of Ref. [42] would help illustrate the point being made in the “Consequences of Contrast Agent Extravasation” section on page 11, it is probably not crucial for the reader’s understanding of our point. In fact, our reference to Fig. 1 in Ref. [36] in the “Basic Contrast Mechanism for DSC-MRI” on page 9 is probably more germane to an appreciation of the fundamentals of susceptibility contrast. We are inclined to keep the number of figures within the recommended guidelines but are happy to add supplemental material should the editor deem it necessary.*

Page 12- good discussion of ferumoxytol. Suggest explicitly adding that this is not widely available.

*The reviewer makes a good suggestion, and we have added the following sentence to the ferumoxytol section on page 12:*

*“FDA-approved as a therapeutic iron supplement, ferumoxytol is less commonly available than GBCA for MRI.”*

Suggest authors consider including a European author to add EU consensus or adoption. Someone like Marion Smits or similar?

*This is an excellent suggestion. We agree that “buy in” from the European community is important, and our author list already includes Marion Smits (representative of the EORTC), as well as neuro-oncologists from Heidelberg, Zurich, and Rotterdam. We also have author representatives from the ABTC, ECOG-ACRIN, Alliance for Clinical Trials in Oncology, and the RTOG, and therefore feel that we stand a very good chance of achieving widespread compliance with our consensus protocol in the US and Europe.*

Although vendors will always have proprietary software, any suggestions to them to implement standard postprocessing steps as outlined in manuscript?

*This is an excellent point raised by the reviewer. Post-processing is very important and impactful for accurate CBV measurements but can be done in many different ways. Variations in post-processing methodology can introduce substantial variability in measured CBV, as demonstrated in Ref. [63]. We believe that it is safe to say that the BSW leakage correction scheme has, by far, the most clinical evidence to support its utility. Furthermore, the DRO work done by Quarles et al. (Ref. [66]) evaluated uncorrected and corrected DSC-MRI data and found that the BSW provided the highest accuracy. For these reasons, we are comfortable suggesting that at this point in time, the BSW method is an advisable technique for performing post-processing model-based leakage correction.*

*However, implementation matters; different vendor implementations of the BSW leakage correction methodology can yield different CBV estimates for the same input data (Ref. [62]). We are obviously not in a position to provide explicit computer code for performing BSW. As we state in our reply to Reviewer #1, it may very well be the case that it will take acceptance of a single CBV analysis software implementation by the neuro-oncology community for widespread use with reproducible results to be achieved, similar to the acceptance of IschemaView RAPID software for thrombectomy trials by the interventional neuroradiology community. In the absence of this, a benchmark may be required for validating DSC-MRI post-processing tools, such as the DRO methodology referenced in our manuscript (Ref. [66]). In such a scenario, vendors could “test”*

*their post-processing implementations against a “gold standard” to ensure that accurate results are obtained.*

*To this end, we have added the following paragraph to the Summary of Updated Recommendations section at the end of the manuscript:*

*“Post-processing leakage correction is beneficial, even for low FA (30°) acquisitions, and should be utilized in routine practice. The BSW method is an advisable technique for performing post-processing model-based leakage correction and has thus far the most computer simulation and clinical evidence to support its utility. In the absence of universal acceptance of a single software implementation for widespread use, a benchmark may be required for validating independent DSC-MRI post-processing tools, such as the DRO methodology referenced above.”*

There is also significant heterogeneity introduced by operator training and measurement techniques. Any consensus recommendations for this? Small fixed ROIs? Or whole lesion VOIs? Histograms? This is the other major impediment to generalizability of DSC MRI in trials and across sites.

*These are all excellent questions raised by the reviewer. For the reasons specified in our response to the second issue raised by Reviewer #1, we have focused this manuscript on consensus recommendations for the DSC-MRI acquisition protocol (i.e., particulars of the DSC-MRI CBV map generation process), including contrast agent dosing, MRI acquisition parameters, and post-processing of the DSC-MRI signal. We have therefore purposefully avoided discussion of CBV analysis tools and methodologies. These are very important issues and would merit their own consensus recommendations.*

### **Reviewer 3**

The paper by Boxerman et al addresses a critical need for standardization of DSC imaging protocols for brain tumor imaging. The paper is very well written and provides a thorough review of the DSC literature and the challenges associated with DSC and multisite studies. The rationale for the recommendations is clearly explained and justified. I have only a few minor comments.

In particular, while the authors extensively discuss the optimization of the image acquisition protocol, there is considerably less attention paid to the post-processing data analysis and leakage correction. Given the importance of proper leakage correction, as discussed by the authors, it seems that more emphasis and guidance could be given for standardization of the leakage correction method.

*This is an excellent point raised by the reviewer. Please see our response to a similar query raised by Reviewer #2.*



*We placed the major emphasis of this consensus protocol manuscript on the standardization of acquisition parameters because the DSC-MRI data can “only be acquired once.” Post-processing leakage correction is very important for obtaining accurate CBV measures, but the raw signal data can of course be reprocessed as algorithms evolve. In general, historical studies and the computer simulations cited in this manuscript have demonstrated excellent performance of the basic BSW technique modified for T2\* correction using full-range K2 fitting. This would seem to be a reasonable proposal for a standardization of the leakage correction method. Implementations will vary, and benchmark datasets for ensuring the accuracy of different implementations would be helpful.*

While it is likely beyond the scope of this manuscript it might also be instructive to point out that the BSW method corrects only for T1 effects of extravasated contrast agent and not T2\* effects of extravasated contrast. In some subjects the leakage can be so severe that T1 correction is not sufficient. Bjonerud et al tried to account for the T2\* contribution of extravasated contrast agent by allowing the K2 leakage term to assume negative or positive values [1], while Mouridsen et al presented an abstract at the 2010 ISMRM Workshop on Improving Cancer Treatment with Advanced MR demonstrating a model that included T2\* effects from extravasated contrast [2]. The K2 leakage parameter that included both T1 and T2\* leakage effects was shown to demonstrate a very similar tumor rim enhancement/leakage as observed in the DCE Ktrans map, while no such enhancement was observed in the K2 map that included only T1 correction. This again suggests that care must be taken for very leaky tumors where T2\* effects from extravasated contrast agent can contribute significantly and the BSW correction method can fail.

1. A Bjonerud, AG Sorensen, K. Mouridsen, KE Emblem. T1- and T2\*-dominant extravasation correction in DSC-MRI: Part I - theoretical considerations and implications for assessment of tumor hemodynamic properties. J Cereb Blood Flow Metab 2011;31;2041-2053.
2. K Mouridsen, CT Farrar, D Jennings, K Emblem, AG Sorensen. DSC Correction for T1 and T2\* Relaxation Induced by Extravasated Contrast Agent. ISMRM Cancer Workshop 2010.

*We thank the reviewer for these insightful comments regarding the T1 and T2\* correction in the BSW correction method. It is our understanding that most commercial systems that employ BSW, including the IB Neuro (Imaging Biometrics) implementation that was used for the in vivo comparison of the low FA, no preload and intermediate FA, full-dose preload schemes (Ref. [82]) do correct for both T1 and T2\* effects by allowing K2 to either be positive or negative, as was done in the Bjonerud paper referenced above. Furthermore, the DRO simulation studies performed by Quarles et al. (Ref. [66]) employed this strategy and found very high accuracy of the corrected CBV using the optimal acquisition parameters. We definitely agree that care must be taken for very leaky tumors where T2\* effects from extravasated contrast agent can contribute significantly, and the original unmodified BSW correction method can fail. We*

*have added reference to the Bjonerud paper on page 14 when stating that modifications to the original BSW method have been subsequently introduced to correct  $T2^*$  leakage effects as well.*

**Consensus Recommendations for a Dynamic Susceptibility Contrast MRI  
Protocol for Use in High-Grade Gliomas**

Jerrold L. Boxerman<sup>1,¥,Ω,£</sup>, Chad C. Quarles<sup>2</sup>, Leland S. Hu<sup>24,◇,Ω</sup>,  
Bradley J. Erickson<sup>3,◇,æ,Ω</sup>, Elizabeth R. Gerstner<sup>4,†</sup>, Marion Smits<sup>5,β</sup>,  
Timothy J. Kaufmann<sup>3,◇</sup>, Daniel P. Barboriak<sup>6,¥,æ,Ω</sup>, Raymond H. Huang<sup>8,9</sup>,  
Wolfgang Wick<sup>10,β</sup>, Michael Weller<sup>11,β</sup>, Evanthia Galanis<sup>12,◇</sup>,  
Jayashree Kalpathy-Cramer<sup>13</sup>, Lalitha Shankar<sup>14</sup>, Paula Jacobs<sup>14</sup>, Caroline Chung<sup>15,◇</sup>,  
Martin J. van den Bent<sup>16,β</sup>, Susan Chang<sup>17</sup>, W.K. Al Yung<sup>18</sup>, Timothy F. Cloughesy<sup>19,20</sup>,  
Patrick Y. Wen<sup>9,†</sup>, Mark R. Gilbert<sup>21,¢</sup>, Bruce R. Rosen<sup>13</sup>,  
Benjamin M. Ellingson<sup>19,22,†,§,¥,æ,Ω</sup>, and Kathleen M. Schmainda<sup>23,¥</sup>

and the Jumpstarting Brain Tumor Drug Development Coalition  
Imaging Standardization Steering Committee

Affiliations:

<sup>1</sup> Department of Diagnostic Imaging, Warren Alpert Medical School, Brown University, Providence, RI

<sup>2</sup> Department of Neuroimaging Research & Barrow Neuroimaging Innovation Center, Barrow Neurological Institute, Phoenix, AZ

<sup>3</sup> Department of Radiology, Mayo Clinic, Rochester, MN

<sup>4</sup> Department of Neurology, Massachusetts General Hospital, Harvard Medical School, Boston, MA

<sup>5</sup> Department of Radiology and Nuclear Medicine, Erasmus MC – University Medical Center Rotterdam, Rotterdam, Netherlands

<sup>6</sup> Department of Radiology, Duke University School of Medicine, Durham, NC

<sup>8</sup> Department of Radiology, Brigham and Women's Hospital, Boston, MA

<sup>9</sup> Center for Neuro-Oncology, Dana-Farber/Brigham and Women's Cancer Center, Harvard Medical School, Boston, MA

<sup>10</sup> Department of Neurooncology, National Center of Tumor Disease, University Clinic Heidelberg, Heidelberg, Germany

<sup>11</sup> Department of Neurology, University Hospital and University of Zurich, Zurich, Switzerland

<sup>12</sup> Division of Medical Oncology, Department of Oncology, Mayo Clinic, Rochester, MN

<sup>13</sup> Martinos Center for Biomedical Imaging, Massachusetts General Hospital and Harvard Medical School, Boston, MA

<sup>14</sup> Division of Cancer Treatment and Diagnosis, National Cancer Institute (NCI), Bethesda, MD

<sup>15</sup> Department of Radiation Oncology, The University of Texas MD Anderson Cancer Center, Houston, TX

<sup>16</sup> Department of Neuro-Oncology, Erasmus MC Cancer Institute, Rotterdam, Netherlands

<sup>17</sup> Department of Neurological Surgery, University of California – San Francisco, San Francisco, CA

<sup>18</sup> Department of Neuro-Oncology, Division of Cancer Medicine, The University of Texas MD Anderson Cancer Center, Houston, TX

<sup>19</sup> UCLA Neuro-Oncology Program & UCLA Brain Tumor Imaging Laboratory (BTIL), David Geffen School of Medicine, University of California – Los Angeles, Los Angeles, CA

<sup>20</sup> Department of Neurology, David Geffen School of Medicine, University of California – Los Angeles, Los Angeles, CA

<sup>21</sup> Neuro-Oncology Branch, National Cancer Institute (NCI), Bethesda, MD

<sup>22</sup> Departments of Radiological Sciences, Psychiatry, and Biobehavioral Sciences, David Geffen School of Medicine, University of California – Los Angeles, Los Angeles, CA

<sup>23</sup> Department of Biophysics, Medical College of Wisconsin, Milwaukee, WI

<sup>24</sup> Department of Radiology, Mayo Clinic, Arizona

Additional Affiliations:

<sup>†</sup> Representative of the Adult Brain Tumor Consortium (ABTC)

<sup>§</sup> Representative of the Ivy Consortium for Early Phase Clinical Trials

¥ Representative of the Eastern Cooperative Oncology Group – American College of Radiology Imaging Network (ECOG-ACRIN) Cancer Research Group

ß Representative of the European Organization for Research and Treatment of Cancer (EORTC)

◇ Representative of the Alliance for Clinical Trials in Oncology

æ Representative of the RSNA Quantitative Imaging Biomarker Alliance (QIBA)

Ω Representative of the American Society of Neuroradiology (ASNR)

£ Representative of the American Society of Functional Neuroradiology (ASFNR)

¢ Representative of the Radiation Therapy Oncology Group (RTOG)

**Corresponding author:** Jerrold L. Boxerman, MD, PhD

Rhode Island Hospital, Department of Diagnostic Imaging

593 Eddy Street

Providence, RI 02903

(401) 444-5184 (Phone)

(401) 444-5017 (Fax)

*jboxerman@lifespan.org*

## Abstract

Despite the widespread clinical use of dynamic susceptibility contrast (DSC) MRI ~~and evidence for its impact on the management of brain tumor patients~~, DSC-MRI methodology has not been standardized, hindering its utilization for ~~treatment~~-response assessment in multi-center trials. Recently, the DSC-MRI Standardization Subcommittee of the Jumpstarting Brain Tumor Drug Development Coalition ~~used~~ issued recommendations by the ASFNR as a springboard for an updated consensus DSC-MRI protocol compatible with BTIP, the standardized ~~MRI~~ brain tumor imaging protocol (~~BTIP~~) for high-grade gliomas that is increasingly used in the clinical setting and. ~~BTIP~~ is the default MRI protocol for the ~~NCI's~~ National Clinical Trials Network ~~and is increasingly used in the clinical setting~~. After reviewing the basis for controversy over DSC-MRI protocols, this manuscript provides evidence-based best practices for clinical DSC-MRI as determined by the Committee, including pulse sequence (gradient echo vs. spin echo), BTIP-compliant contrast agent dosing (preload and bolus), flip angle (FA), echo time (TE), and post-processing leakage correction. In summary, full-dose preload, full-dose bolus dosing using intermediate (60°) FA and field strength-dependent TE (40-50ms at 1.5T, 20-35ms at 3T) provides overall best accuracy and precision for cerebral blood volume estimates, ~~reiterating findings by the ASFNR~~. When single-dose contrast agent usage is desired, no-preload, full-dose bolus dosing using low FA (30°) and field strength-dependent TE provides excellent performance, with reduced contrast agent usage and elimination of potential systematic errors introduced by variations in preload dose and incubation time ~~and dose allocation between preload and bolus administrations~~.

**Keywords:** DSC-MRI; cerebral blood volume; high-grade glioma; clinical trial; consensus protocol



## Introduction

In 1990, Rosen et al. demonstrated transiently decreased brain signal intensity after bolus administration of gadolinium-based contrast agent (GBCA).<sup>1</sup> The signal intensity-time curve could be converted into a concentration-time curve, enabling voxel-wise computation of cerebral blood volume (CBV). This technique, now widely known as dynamic susceptibility contrast (DSC) MRI, uses the magnetic susceptibility properties of paramagnetic contrast agents (gadolinium chelates or superparamagnetic nanoparticles) and T2 or T2\*-weighted acquisitions. DSC-MRI was used to perform the first “functional” MRI experiments of task-induced brain activation,<sup>2</sup> and produce the first MRI-based CBV maps of gliomas.<sup>3</sup>

Since these beginnings, studies have shown that DSC-MRI may be more useful than standard MRI at predicting treatment-naïve glioma grade<sup>3-8</sup> and survival,<sup>9-13</sup> distinguishing post-treatment pseudoprogression and radiation necrosis from recurrent tumor,<sup>14-17</sup> and predicting response to anti-angiogenic therapy.<sup>18-25</sup> Use of DSC-MRI has consequently exploded over the past few decades, particularly in neuro-oncology. Geer et al. found that the addition of DSC-MRI increased the confidence of neuroradiologists and treating physicians in their assessment of tumor status in 40% and 56% of cases, respectively, with treatment modification in 8.5% of patients,<sup>26</sup> highlighting the potential clinical impact of DSC-MRI. Despite this and other evidence for clinical impact on the management of brain tumor patients, technical aspects of DSC-MRI have not been standardized, which has hindered its widespread adoption and utilization for assessment of treatment response in multi-center therapeutic trials.

There are multiple protocol decisions for DSC-MRI that influence its practical implementation and the accuracy and precision of CBV measurement.<sup>27</sup> These include gradient echo (GRE) versus spin echo (SE) pulse sequence; contrast agent dosing, including preload and bolus; image acquisition parameters, including flip angle (FA), echo time (TE), temporal resolution (TR) and number of baseline and post-bolus data points; and post-processing techniques, including GBCA leakage correction. After reviewing the basis for controversy over DSC-MRI protocol, this manuscript provides *evidence-based best practices for clinical DSC-MRI*, emphasizing our favored choices for these protocol decisions. The *evidence* comes from DSC-MRI theory, computer modeling and simulation of DSC-MRI signal acquisition and post-processing, in vivo stereotactic tissue correlation, and single-institution and multi-site clinical trial data. Because a primary goal for harmonizing DSC-MRI methodology is the facilitation of its widespread adoption and the collation of results from multi-site trials, for *best clinical practice* we emphasize CBV *accuracy* and *precision* in neuro-oncology applications, including treatment response assessment of high-grade gliomas in clinical trials of novel therapeutics. Although advanced DSC-MRI methods including multi-echo approaches may measure additional features of tumor pathophysiology (including vessel caliber, vascular permeability, tumor cell size and cytoarchitecture),<sup>28,29</sup> our recommendations focus on CBV measurement using single TE, GRE echo planar imaging and GBCA-based DSC-MRI, which is the most common methodology in practice and is concordant with other widely adopted brain tumor imaging protocols.<sup>30</sup>

## A Brief Overview of DSC-MRI

DSC-MRI is based upon classical indicator dilution theory used by physiologists to quantitate hemodynamics of whole-organ systems from known quantities of injected non-diffusible tracers such as dyes and radiotracers, and measurement of output tracer concentration.<sup>31</sup> DSC-MRI applies this methodology to the brain, using exogenous paramagnetic GBCA as the “tracer”. DSC-MRI is a “bolus tracking” technique that rapidly acquires GRE or SE echo planar images before (baseline), during (bolus), and after (tail) first-pass transit through the brain of GBCA that transiently alters the acquired signal intensity.<sup>32</sup> Voxel-wise changes in relative contrast agent concentration are determined by converting the signal intensity-time curves into change in relaxation rate-time curves, assuming that transient signal loss is due solely to magnetic susceptibility effects resulting from the injected GBCA and the subsequent changes in  $T2^*$  (GRE) or  $T2$  (SE) relaxation rate ( $\Delta R2^*$  and  $\Delta R2$ , respectively, and herein referred to collectively as  $\Delta R2^*$  unless otherwise specified). Because  $\Delta R2^*$  is assumed to be directly proportional to tissue GBCA concentration, with GBCA confined to the vasculature, the  $\Delta R2^*$ -time curves are processed using tracer kinetic modeling and indicator dilution theory to estimate cerebral hemodynamic parameters such as CBV, cerebral blood flow (CBF), and mean transit time (MTT).<sup>1</sup> Absolute CBV can theoretically be determined from the area under the  $\Delta R2^*$ -time curve normalized to the integrated arterial input function (AIF).<sup>33</sup> Most often, to avoid the well-known difficulties of accurately determining the AIF, relative CBV (rCBV) is estimated from the area under the  $\Delta R2^*$ -time curve alone giving a CBV value that has meaning relative to other parts of the brain. For comparison across time and patients, rCBV may be normalized to rCBV in normal-appearing white matter, yielding the most

common DSC-MRI metric for evaluating brain tumors, normalized rCBV (nRCBV). Alternative methods precluding the need to normalize rCBV to reference brain include standardization and Gaussian normalization.<sup>34,35</sup>

## **Basic Contrast Mechanism for DSC-MRI**

The DSC-MRI contrast mechanism is based upon compartmentalization of paramagnetic GBCA that establishes magnetic susceptibility difference between the intra- and extra-vascular space, creating magnetic field gradients.<sup>32</sup> Protons lose phase coherence as they diffuse through the transient, spatially varying gradients, yielding signal attenuation dependent upon physiological factors, including vessel or compartment size and proton diffusion rate, and experimental factors, including pulse sequence parameters and contrast agent concentration.<sup>36</sup> Although this behavior can be solved analytically for limited regimes, this phenomenon has been most generally studied using Monte Carlo numerical methods that quantify the relationship between change in relaxation rate and the physiological and experimental parameters.<sup>36,37</sup> These simulations yield the vessel size-dependence relationships for GRE ( $\Delta R2^*$ ) and SE ( $\Delta R2$ ) change in relaxation rate, with  $\Delta R2^*$  plateauing for large diameter vessels, and  $\Delta R2$  peaking for capillary-sized vessels (e.g., Figure 1 in Ref. [36]). These relationships are qualitatively independent of vessel geometry.

## **Gradient-echo versus Spin-echo Acquisitions**

The vessel size-dependence relationships have clinical implications. Because  $\Delta R2$  peaks for microvessels, SE DSC-MRI is advantageous in stroke imaging aimed at

identifying capillary-level perfusion deficits,<sup>38</sup> with reduced blooming artifact in cortex around sulcal vessels. GRE DSC-MRI is sensitive to the larger, disorganized vessels that characterize high-grade gliomas,<sup>39,40</sup> with obvious application to tumor imaging. For given contrast agent concentration, field strength, and imaging parameters,  $\Delta R2^*$  exceeds  $\Delta R2$  for all vessel sizes, with larger corresponding signal loss.<sup>36</sup> Therefore, GRE-derived CBV maps have higher inherent SNR and sensitivity than SE CBV maps, and can provide greater signal changes for equal GBCA dose, or equivalent signal changes with lower GBCA dose, compared to those derived with SE DSC-MRI.

In order for DSC-MRI to accurately measure cerebral hemodynamics, there must be a linear relationship between change in relaxation rate and GBCA concentration. From basic susceptibility contrast principles, change in relaxation rate is directly proportional to GBCA concentration only where the  $\Delta R2$  or  $\Delta R2^*$  versus vessel size curves are “plateaued”.<sup>41</sup> This plateau occurs over a much broader range of vessel sizes for GRE ( $\Delta R2^*$ ) compared to SE ( $\Delta R2$ ) DSC-MRI, and so GRE CBV estimates are inherently more accurate than SE CBV estimates. Similarly, the  $x$ -axis of the size-dependence curves actually scales as  $R^2/D$ , where  $R$  is the vessel size and  $D$  is the proton diffusion rate.<sup>41</sup> Therefore, decreasing  $D$  (restricted diffusion) has the same effect as increasing vessel size (moving to the right on the change in relaxation rate versus vessel size graphs). While increasing vessel diameter or decreasing diffusion can result in either increased or decreased  $\Delta R2$ ,  $\Delta R2^*$  will be much less affected because of the plateau in the  $\Delta R2^*$ -size curve. Therefore, in tumors with heterogeneous proton diffusion and abnormal vascular morphology, hyperintensity on CBV maps is more likely to reflect truly elevated blood volume for GRE acquisitions versus greater uncertainty for SE acquisitions.

For these reasons – sensitivity to larger, disorganized microvessels seen in higher-grade tumors; greater signal changes for a given contrast agent dose; greater inherent accuracy of CBV estimates; and decreased sensitivity to changes in proton diffusion – GRE DSC-MRI is recommended for neuro-oncology applications. Thus, moving forward, we will only refer to T2\* changes that occur with GRE DSC-MRI.

## **Consequences of Contrast Agent Extravasation**

Another requirement for DSC-MRI to mimic tracer kinetics is that contrast agent must remain intravascular, which is violated for GBCAs in high-grade gliomas (HGG) with blood-brain barrier (BBB) disruption and avid contrast enhancement. GBCA extravasation results in T1 shortening, opposing the susceptibility contrast induced T2\* relaxation rate change from intravascular GBCA that forms the basis for CBV estimation. Because GBCA is excluded from cells, GBCA extravasation establishes a magnetic susceptibility gradient not only between the intra- and extra-vascular spaces, but also between the intra- and extra-cellular spaces when sufficient GBCA distributes throughout the extravascular-extracellular space, potentially exaggerating T2\* changes. (As an example see Figure 5 of Ref. [42] where in the same voxel the post-bolus signal can overshoot or undershoot baseline depending upon the accumulated dose of GBCA.) DSC-MRI signal is thereby affected not only by vascular volume fraction and vessel size, but also by the rate of GBCA extravasation (vascular permeability) and the cell volume fraction, cell size and cell distribution.<sup>28</sup> Signal-time (and  $\Delta R2^*$ -time) curves no longer return to baseline as they do for ideal tracer kinetics, but extend below or above baseline depending on whether T1 or T2\* effects dominate, thereby affecting the accuracy of CBV estimates determined from

the area under the  $\Delta R2^*$ -time curve.<sup>43</sup> The magnitude of this effect depends upon a combination of both DSC-MRI acquisition parameters and contrast agent dosing.<sup>42</sup>

Methods for minimizing DSC-MRI signal contamination from GBCA extravasation include low FA pulse sequences that reduce T1 sensitivity;<sup>44</sup> loading doses or “preload” contrast administration;<sup>5,8,45</sup> and post-processing techniques including model-based leakage correction that can rectify both T1 and T2\* leakage effects.<sup>5,8,45-47</sup> Dual-echo DSC-MRI utilizes two GRE acquisitions with different TEs to estimate change in relaxation rate directly, thereby eliminating T1 contamination effects entirely, but still requires correction for T2\* leakage effects<sup>48</sup> and special pulse sequences that are less widely available.<sup>38,49</sup> No technique has been universally accepted, and much of the debate about best DSC-MRI methodology centers on issues related to minimizing contamination of the DSC-MRI signal due to GBCA extravasation and maximizing CBV accuracy.

Intravascular contrast agents like ferumoxytol eliminate contrast agent leakage effects entirely, and there is compelling evidence that ferumoxytol-based CBV measurements are inherently more accurate and precise than gadolinium-based CBV measurements because complications related to GBCA extravasation are minimized.<sup>50</sup> However, clinical application of ferumoxytol-based DSC-MRI may be limited. FDA-approved as a therapeutic iron supplement, ferumoxytol is less commonly available than GBCA for MRI. GBCAs are widely accepted by radiologists for conventional post-contrast imaging and adding a second contrast agent for DSC-MRI would be logistically challenging. Although conventional contrast-enhanced imaging is feasible with ferumoxytol, it is practically performed 24 hours after agent administration.<sup>51</sup> Furthermore, the standardized BTIP requires post-contrast imaging after one total dose

of GBCA.<sup>30</sup> Finally, gadolinium-based DSC-MRI permits measurement of additional physiological parameters related to GBCA extravasation, such as PSR (percent signal recovery of the signal-time curve compared to baseline), as well as  $K^{trans}$  (volume transfer coefficient of gadolinium from the intravascular to the extravascular, extracellular space). Therefore, we focus on single-GRE GBCA-based DSC-MRI and the selection of four fundamental protocol choices: preload and bolus contrast agent dose, FA, TE, and post-processing leakage correction.

## Preload Contrast Agent Dosing

A “preload” dose of GBCA administered prior to the bolus dose of GBCA given during dynamic imaging can help mitigate T1 contamination. The preload dose partially saturates baseline T1-weighted signal contribution,<sup>5,8,45</sup> thereby diminishing T1-induced increased signal during bolus passage. Evidence supporting preload administration includes data in a C6 rat glioma model, where (at least for high-FA acquisitions) there is no discernable DSC-MRI signal after the first (no preload) injection, and a “usable” DSC-MRI signal for computing CBV with the second injection.<sup>46</sup> A study comparing several different approaches for acquiring and computing rCBV maps in patients demonstrated that without preload, high-grade tumor may mistakenly show no rCBV elevation compared to normal brain, but expected rCBV elevation is found when a preload was used.<sup>42</sup> Preload dosing has varied in the literature, ranging from fractional doses up to a full equivalent dose. In a study using a 60° FA and post-processing leakage correction, Hu et al. found that a full-dose preload of 0.1 mmol/kg and an incubation time of 6 minutes between preload administration and bolus injection optimized the separation of CBVs for



tumor and treatment effect in HGGs with recurrent enhancement after standard chemoradiation.<sup>52</sup>

## Post-Processing Leakage Correction

In practice, DSC-MRI acquisition cannot be decoupled from post-processing, and there is ample evidence that post-processing leakage-correction of DSC-MRI data is necessary for accurate rCBV measurement when the BBB is disrupted.<sup>5,8,45</sup> A pharmacokinetic model-based approach described by Weisskoff et al.<sup>53</sup> was the first published method for correcting T1-based GBCA leakage effects using a linear least-squares fit of the  $\Delta R2^*$ -time curves within the tumor and a reference region in non-enhancing brain to correct the entire  $\Delta R2^*$ -time curve, including first pass.<sup>5,8,45,46</sup> The method was subsequently modified to correct T2\* leakage effects as well,<sup>45,54</sup> and it was empirically determined that the algorithm performed best with the collection of 120 time points, a finding consistent with the assumption of no contrast agent backflux. This leakage correction method is now sometimes referred to as the BSW method (after the authors of the subsequent paper that focused exclusively on the leakage correction algorithm<sup>8</sup>).

Modifications to the BSW approach have since been published, including calculation of the tissue residue function allowing for a voxel-wise correction of the raw DSC-MRI signal that is insensitive to variations in MTT.<sup>46</sup> The ability to determine additional perfusion parameters directly from the residue function has also been demonstrated.<sup>54</sup> Most recently, a “bidirectional” version of the BSW method was developed that accounts for backflux of contrast agent,<sup>47,55</sup> which becomes important with

the collection of >120 time points. While other leakage correction methods like gamma-variate fitting and post-bolus baseline correction have been used, studies suggest that these do not perform as well because they do not correct for leakage effects occurring throughout the DSC bolus.<sup>42,46</sup>

Preload and model-based post-processing leakage correction are synergistic in their improvement of rCBV accuracy,<sup>42</sup> and consensus recommendations for leakage-corrected, single-echo DSC-MRI have been directed towards a technique combining the two methods.<sup>56</sup> For high FA, rCBV using preload plus leakage correction strongly correlates with tumor grade, whereas uncorrected rCBV does not,<sup>8</sup> and in a rat gliosarcoma model, combined preload and post-processing leakage correction yield CBV estimates that converge to gold standard values obtained using MION, an intravascular contrast agent.<sup>57</sup> RCBV measurements using preload and the BSW method agree well with histology in spatially correlated tissue biopsies,<sup>58,59</sup> and the BSW method has been applied in single-institution studies and multi-site clinical trials demonstrating, among other benefits, the utility of rCBV for predicting or detecting early responses to therapy.<sup>20,23,60,61</sup> Nonetheless, there are potentially important improvements to be gained using modified BSW approaches that have yet to be thoroughly evaluated.

Although the BSW method has been implemented by several commercial software vendors, discrepancies in computed rCBV arise in head-to-head comparisons,<sup>62</sup> and caution is recommended for cross-platform comparisons. For instance, significantly different performance was observed when identical DSC-MRI data were processed with two software packages using different implementations of post-processing leakage correction.<sup>62</sup> The best correlation of CBV with histology required preload plus post-

processing leakage correction, providing evidence that leakage correction is important but that technique and implementation matter. Marked inter-site disagreement has also been observed when site-specific software was applied to DSC-MRI data generated by a digital reference object (DRO) using a standardized imaging protocol.<sup>63</sup> Nonetheless, it has been shown that when a single data set is carefully pre-processed eliminating differences in intermediate analysis steps (such as ROI selection and registration), then rCBV values computed by multiple sites using different platforms begin to converge,<sup>64</sup> and a “consensus” threshold is reached for distinguishing low-grade from high-grade gliomas. Therefore, implementation matters, motivating efforts to build consensus regarding post-processing and to establish a benchmark for validating DSC-MRI analysis tools, such as the DRO described below.<sup>65,66</sup>

## **Impact of Flip Angle and TE**

For single-echo DSC-MRI, low to intermediate FA (i.e. 35°–60°) with longer TR (i.e. 1.2–1.7s) and TE (i.e. >20ms) can reduce T1 contamination due to GBCA extravasation.<sup>44</sup> However, some parameter combinations may also reduce the SNR of the computed rCBV maps,<sup>67</sup> and the goal is to minimize leakage effects while maintaining SNR. Accordingly, there are high- and low-FA DSC-MRI strategies with tradeoffs, as summarized in Table 1. Acquisitions using low FA,<sup>44</sup> long TE,<sup>68</sup> and long TR<sup>69</sup> have decreased T1 sensitivity, and less need for preload, but poorer CBV SNR. Higher FA,<sup>8</sup> shorter TE,<sup>70</sup> and shorter TR<sup>67</sup> may require preload to decrease T1 sensitivity, but have higher CBV SNR.

We have direct validation of CBV accuracy using two different acquisition strategies. Stereotactic biopsies co-registered to leakage-corrected CBV maps made with

preload, 60° FA, and post-processing leakage correction have shown excellent correlation of CBV with histologic vascular area and density.<sup>58</sup> Similarly, stereotactic biopsies co-registered to CBV maps made using no preload, a low FA (35°), and no model-based leakage correction also had good correlation of CBV with microvascular expression.<sup>71</sup> The literature is replete with conflicting acquisition strategies such as these.

## **Motivation for Standardization of DSC-MRI Methodology**

The application of DSC-MRI to treatment response assessment of HGGs illustrates the importance of harmonization of DSC-MRI methodology. There has been much investigation of the use of CBV for differentiating true tumor from treatment effects. Relative CBV has putative value for differentiating progressive disease (PD) characterized by enlarged microvessels with high vascular density from treatment effects characterized by inflammatory or steroid-like behavior as in pseudoprogression (PsP) or pseudoresponse, respectively.<sup>72-74</sup>

CBV has been used to distinguish PsP and PD at initial progressive contrast enhancement after chemoradiation but the literature is somewhat conflicting. For instance, Prager et al. studied 68 HGGs at progressive enhancement and found significant difference in median rCBV between PsP and PD, with an optimal threshold of 1.3.<sup>75</sup> Other studies also found mean or median CBV to be predictive, with varying thresholds,<sup>19,76</sup> but others have found mean CBV to be non-predictive or only predictive with qualification. Although Kong et al. found overall significant difference in mean rCBV between PsP and PD, this difference applied to GBMs with unmethylated but not with methylated MGMT.<sup>77</sup> However, a study of HGGs treated with PPX, a powerful radiation sensitizer with a high incidence of PsP often coincident with PD, found no significant

difference in mean rCBV between PsP and PD at initial progressive enhancement.<sup>78</sup>

These are just a few examples of varied results in the literature.

## **Variability of DSC-MRI Methodology in the Literature**

Literature results may conflict at least in part because DSC-MRI methodology varies greatly. Patel et al. published a meta-analysis of 17 studies where DSC-MRI was used to differentiate recurrent HGG from treatment-related enhancement.<sup>79</sup> For the subgroup of studies using mean lesion rCBV, they found “relatively good accuracy in individual studies” with high pooled sensitivity (88% [0.81-0.94]) and specificity (88% [0.78-0.95]) for recurrent tumor, but there was a wide range of optimal mean CBV thresholds (0.9–2.15). This variation has been attributed to the wide range of TR, TE, FA, preload dose and post-processing leakage correction used by these studies, as summarized in Figure 1. Variable parameters are also found in subsequent literature. For instance, using spatially correlated histologic tissue samples, TR = 1100-1250ms, TE = 30ms, FA = 70-80°, ½-1 dose preload with full-dose bolus, and post-processing leakage correction (IB Neuro™), Prah et al. found a nRCBV cutoff of 1.13 with 82% sensitivity and 90% specificity.<sup>59</sup> Patel et al. concluded that “because of significant variability in optimal reported thresholds...further investigation and standardization is needed before implementing any particular quantitative PWI strategy across institutions.”

On a similar note, Quarles et al. organized a Quantitative Imaging Network (QIN) DSC-MRI challenge with 12 NCI-QIN centers to explore factors related to CBV consistency.<sup>63</sup> They simulated a 10,000-voxel population-based DRO for each site’s DSC-MRI protocol (19 total protocols),<sup>65</sup> and used corresponding DSC-MRI signal curves

for three evaluations of inter-site CBV consistency: central processing of CBV for site-specific DROs (isolated impact of acquisition protocol); site-specific processing of CBV for standard DRO (isolated impact of post-processing methodology); and site-specific processing of CBV for site-specific DROs (combined impact of acquisition and post-processing). The 3T DSC-MRI acquisition protocol varied considerably for the 12 sites (15 paradigms). Though TR and TE were relatively consistent (possibly reflecting adoption of previously published protocol recommendations<sup>56</sup>), FA and preload dosing varied considerably, with a wide gamut of post-processing methodology, including software, integration limits, and normalization to white matter. When local sites chose both acquisition and post-processing, there was very poor cross-site intra-class correlation for CBV, particularly for simulated blood-brain barrier disruption typical for GBMs, and with large limits of agreement on Bland-Altman analysis. There was better correlation when acquisition or post-processing was standardized, especially post-processing. Overall, this study demonstrates that CBV variability can arise from differences in post-processing as well as image acquisition. This has profound implications for comparing literature CBV values from sites using dissimilar acquisition and post-processing schemes. For clinical trials, although acquisition and post-processing methods are typically standardized, the most accurate and proven approaches should be used for determining the therapeutic effectiveness of a drug, or establishing thresholds for categorical response (e.g., predetermined changes in CBV used to refine RANO criteria).

## **Previous Efforts at Standardization: ASFNR White Paper (2015)**

Efforts at standardization have been made by several organizations including the ASFNR, which published a white paper with the following recommendations: single-echo, GRE pulse sequence; TR = 1.0-1.5s; TE = 40-45ms at 1.5T, 25-35ms at 3T; FA = 60-70°; acquisition duration of at least 120 total time points, including at least 30-50 baseline acquisitions; and ¼-1 dose preload with full-dose bolus.<sup>56</sup> These recommendations were made prior to the publication of the standardized BTIP,<sup>30</sup> which is gaining clinical acceptance.

## **BTIP Compliance and Implication for Allowable Dosing Schemes**

It is sensible that a standardized DSC-MRI protocol be compatible with BTIP. BTIP mandates that conventional post-contrast T1-weighted imaging be performed after one full dose of GBCA, either split between preload and DSC-MRI bolus before post-contrast imaging, or fully given as preload with variable bolus dose DSC-MRI after post-contrast imaging. This sets constraints on the range of preload and bolus doses that should be considered for inclusion in a universal DSC-MRI protocol. Possible BTIP-compliant DSC-MRI preload and bolus paradigms are illustrated in Figure 2.

## **Selection of Optimal DSC-MRI Parameters: Computational Approach**

Because it is impractical to compare all possible acquisition schemes in vivo, computational approaches have been pursued for determining optimal acquisition parameters.

Using a multi-compartment model-based simulation of DSC-MRI signal derived from convolution theory,<sup>80</sup> the theoretical framework developed by Quarles et al.,<sup>43</sup> and characteristics from 250 randomly chosen tumors, Leu et al. systematically evaluated the effects of various acquisition and post-processing leakage correction strategies, including a range of FA, TE, and TR with BTIP-compliant contrast agent dosing schemes, on the fidelity of CBV estimation in the presence of Gaussian noise.<sup>81</sup> Results of this comprehensive study are summarized in Figure 3. Although no single acquisition scheme was absolutely optimal, several parameter combinations yielded the lowest error in CBV estimation. The best performing acquisition schemes included 60° FA with full-dose preload and full-dose bolus (“1+1” double-dose GBCA), as well as 35° FA without preload. Importantly, high-FA acquisitions with no or fractional preload dosing performed relatively poorly.

Similarly, Semmineh et al. used a validated population-based DRO, derived from 3D tumor tissue microstructures and trained on 23 DSC-MRI glioblastoma datasets including more than 40,000 voxels.<sup>65</sup> They simulated tumor CBV acquired with BTIP-compliant dosing schemes, and a similar range of FA, TE, and TR. Simulated CBV without leakage was the reference standard, and they evaluated concordance correlation coefficient and coefficient of variation as measures of accuracy and precision, respectively. They produced heat maps with similar findings as Leu et al. The best performing schemes used full-dose preload and full-dose bolus at low to intermediate FA, with poor performance for intermediate-high FAs using no or fractional preload, particularly at 1.5 T.<sup>66</sup> Confluent regions of high performance are desirable because these



schemes would presumably be less sensitive to minor parameter variations or to underlying model assumptions or tumor physiology.

Figure 4 summarizes performance of the intermediate 60° FA scheme from the ASFNR white paper versus a high-performing, low FA scheme for TR=1.5s. Full-dose preload with full-dose bolus (“1+1” double-dose GBCA) provides the highest accuracy and precision for both schemes with similar performance at 1.5 and 3T. With intermediate FA, single total dose schemes have poorer performance, especially at 1.5T, with moderate performance for split dose at 3T. Low FA acquisitions give much better performance for single total dose. For single-dose contrast without preload, the ASFNR parameters (i.e., intermediate FA) perform poorly, but low FA maintains excellent performance, even at 1.5T. Non-BTIP compliant preload dosing (e.g., ½ or ¼ dose) with full-dose bolus can give excellent results with low FA and intermediate FA at 3T, and very good results at 1.5T.

Convergence of results from these simulations suggest that even without preload (i.e., “0+1” dosing), a low FA scheme gives very accurate CBV with much less bias compared to intermediate FA, even at 1.5T, and could be an attractive approach requiring less contrast agent (Figure 5A).

With the application of simultaneous multi-slice or multi-band techniques, it is possible to shorten the temporal resolution to sub-second TRs, while maintaining sufficient spatial coverage. DRO-based recommendations for TR, TE, and FA seek the optimal T1 and T2\* sensitivity, and sub-second TRs will increase sensitivity to T1 leakage effects and reduce rCBV fidelity. For example, the DRO analysis for “0+1” dosing and the optimal low FA approach described above (30° FA, 30ms TE) predicts that the

concordance correlation coefficient (CCC), a measure of CBV accuracy, drops to 0.76 and 0.62 for TR=750ms and 500ms, respectively. Even if TE is increased to 50ms, CBV accuracy is lower ( $CCC < 0.9$ ) than that achieved using more conventional TRs (1–1.5s). However, for “1+1” dosing and the optimal low FA scheme, the CCC exceeds 0.95, even for TRs as low as 500ms. These results highlight the importance of parameter consistency and encourage caution when applying acceleration techniques.

### **In vivo Assessment of Low FA, No Preload DSC-MRI**

A recent study was performed to validate in vivo the simulations predicting that single-dose, low-FA DSC-MRI acquisitions without preload (“0+1” dosing) give rCBV estimates practically equivalent to the double-dose, intermediate-FA reference standard using full-dose preload (“1+1” dosing).<sup>82</sup> 84 patients with a contrast-enhancing brain lesion were included in this four-institution study. As shown in Figure 5B, the study demonstrated practical equivalence between the two methods, supporting the idea that this low-dose approach should be considered for consensus protocol recommendation, at least at 3T. The agreement between the two methods was poor if post-processing leakage correction (BSW method) was not also applied. Confirmation of equivalence at 1.5T requires a similar study.

### **Conclusions from Computational Parameter Analyses and In Vivo Comparison Study**

Based on the recent literature, the following conclusions can be drawn regarding DSC-MRI acquisition methodology:

1) Of the BTIP-compliant dosing schemes investigated, full-dose preload with full-dose bolus (“1+1” dosing) has superior performance, with the least sensitivity to minor pulse sequence parameter fluctuations and the best combination of accuracy and precision, which is important for clinical trials that aim to minimize sample size. Although both low FA (30°) and intermediate FA (60°) sequences provide a high degree of accuracy in simulations testing the “1+1” dosing scheme, we continue to consider intermediate FA (60°) to be the gold standard for “1+1” dosing, particularly at 3T field strength, given the benefits of higher CNR and lower sensitivity to parameter variations (e.g., TE, TR) compared to low FA (30°) acquisitions.

2) When the “1+1” dosing scheme is not desirable (e.g., when prioritizing low GBCA dosage), the no-preload paradigm (“0+1” dosing) with low FA (30°) and an optimally selected and field-strength dependent TE provides an excellent practical alternative to the gold standard and is the recommended alternative method, particularly at 3T for which in vivo validation has been performed. Based on simulation testing of the “0+1” dosing scheme, low FA (30°) acquisitions provide superior accuracy and precision compared to the intermediate FA (60°). This appears to hold true at both 1.5T and 3T field strengths (though has not yet been validated in vivo at 1.5T).

3) For both the “1+1” dosing at intermediate FA (60°) and “0+1” dosing at low FA (30°), there is a modest theoretical performance advantage at 3T versus 1.5T.

4) For BTIP-compliant fractional dosing (e.g., “ $\frac{1}{2}+\frac{1}{2}$ ” and “ $\frac{1}{4}+\frac{3}{4}$ ” dosing schemes), a low FA (30°) acquisition should be used at all field strengths, given the superior accuracy and precision compared to intermediate FA (60°) acquisitions, with TE = 30-50ms having theoretical advantages, especially at 1.5T. However, these fractional dosing schemes

likely have poorer performance than the “0+1” dosing scheme and the gold-standard “1+1” dosing scheme, due to the theoretical costs of poor CNR for fractional bolus dosing, particularly for perfusion metrics such as cerebral blood flow CBF and MTT.

5) Post-processing leakage correction is always beneficial, even for low FA (30°) acquisitions, and should be utilized in routine practice.

## **Time-point specifications**

### Number of baseline time points

Because the number of baseline acquisitions impacts CBV map SNR, image acquisition should begin at least 30–50 time points before contrast injection via a power injector.<sup>67</sup>

### Number of post-bolus time points

Post-processing leakage-correction algorithms and PSR analysis utilize post-bolus “tail” signal intensities, necessitating acquisition of sufficient post-bolus time points. 120 total time points (for a typical TR of 1.0–1.5s) have been shown by simulation to yield optimal results using the BSW post-processing leakage correction methodology and a 30-50 time point baseline.<sup>66</sup> For longer total acquisitions (e.g., 180 time points), reflux of contrast agent back into blood vessels is more likely to occur, violating assumptions of unidirectional contrast agent efflux.<sup>8</sup> In such cases, bidirectional contrast agent leakage correction schemes are more accurate,<sup>47</sup> with similar accuracy for unidirectional and bidirectional leakage correction when 120 total time points are acquired.<sup>66</sup>

## Compatibility with DCE-MRI

When acquisition of both DCE- and DSC-MRI is desired for a single exam, DCE-MRI is typically performed using the preload dose for DSC-MRI. Preload-based, BTIP-compliant dosing strategies that have been previously evaluated include the “1+1” and “ $\frac{1}{2}+\frac{1}{2}$ ” protocols. Due to the higher CNR of full-dose acquisitions, the “1+1” dosing scheme provides superior DCE- and DSC-parameter accuracy and precision. However, as highlighted in Figure 4, the “ $\frac{1}{2}+\frac{1}{2}$ ” protocol with low FA (30°) provides a reasonable alternative with a modest reduction in accuracy and precision. It is important to note that although the DSC-MRI preload could be used for DCE-MRI, dosage needs to be guided by both DCE-MRI requirements and BTIP compliance, and further investigation is required for determining the fidelity and clinical utility for candidate dosing strategies.

## Summary of Updated Recommendations for DSC-MRI Parameters

In light of the emergence of the BTIP standards,<sup>30</sup> recent computer simulation results,<sup>66,81</sup> and multi-site in vivo validation,<sup>82</sup> our committee is proposing several modifications to the previously published ASFNR recommendations. Because adoption of DSC-MRI is anticipated for multi-site trials, our modified DSC-MRI protocol is BTIP-compliant, imposing constraints on contrast agent preload and bolus selection.

From a theoretical perspective, a full-dose preload, full-dose bolus dosing scheme (“1+1”), using low (30°) or intermediate (60°) FA and field strength-dependent TE (40-50ms at 1.5T, 25-35ms at 3T) provides overall best performance based upon accuracy and precision estimates. In clinical trials or at independent clinical sites where double contrast agent dose is acceptable and highest performance is desired, the double-dose

“1+1”) approach can be used. However, when single-dose GBCA usage is desired or required, we recommend a no-preload, full-dose bolus dosing scheme (“0+1”) using low FA (30°) and field strength-dependent TE (40-50ms at 1.5T, 25-35ms at 3T). For most typical applications and with excellent performance preservation, the “0+1” approach has advantages, including reduced GBCA usage, as well as elimination of potential systematic error introduced by variation in incubation time between preload and bolus administrations. Although the no-preload, low-FA scheme has slightly poorer accuracy and precision than the full-dose preload, full-dose bolus scheme, the “1+1” scheme uses more GBCA, and that downside may more than outweigh the slight gain in performance. Even the fractional dosing schemes (“ $\frac{1}{4}+\frac{3}{4}$ ” and “ $\frac{1}{2}+\frac{1}{2}$ ”), with near equivalent performance using low FA, still have the disadvantage of requiring preload, and potential variation in incubation times can lead to systematic errors. Therefore, the no-preload “0+1” protocol may be most appropriate for routine clinical use.

Post-processing leakage correction is beneficial, even for low FA (30°) acquisitions, and should be utilized in routine practice. The BSW method is an advisable technique for performing post-processing model-based leakage correction and has thus far the most computer simulation and clinical evidence to support its utility. In the absence of universal acceptance of a single software implementation for widespread use, a benchmark may be required for validating independent DSC-MRI post-processing tools, such as the DRO methodology referenced above.

The updated DSC-MRI protocol recommendations are summarized in Table 2. Integrated BTIP and DSC-MRI protocols for the “0+1” and “1+1” dosing schemes are summarized in Supplemental Table 1 and Table 2, respectively.

As a final thought, it is worth noting that although the updated DSC-MRI protocol is motivated by theory, computer simulations, in vivo studies, and clinical trial data related to high-grade gliomas, the principles apply to any contrast-enhancing brain lesion, including metastases and active inflammation or infection. Therefore, we believe that the protocol recommendations herein are generally applicable to routine clinical practice.

## **Funding**

U01 CA176110 (KMS), R01 CA 082500 (KMS), Medical College of Wisconsin Cancer Center (KMS), R01 CA221938 (JLB, CCQ, LSH, KMS) R01 CA213158-01 (CCQ), American Cancer Society (ACS) Research Scholar Grant (RSG-15-003-01-CCE) (Ellingson); American Brain Tumor Association (ABTA) Research Collaborators Grant (ARC1700002)(Ellingson); National Brain Tumor Society (NBTS) Research Grant (Ellingson, Cloughesy); NIH/NCI UCLA Brain Tumor SPORE (1P50CA211015-01A1) (Ellingson, Cloughesy); NIH/NCI 1R21CA223757-01 (Ellingson)

## **Acknowledgments**

We would like to thank additional members of the Jumpstarting Brain Tumor Drug Development Coalition Imaging Standardization Steering Committee including David F. Arons and Ann Kingston from the National Brain Tumor Society (NBTS), Boston, MA, David Sandak and Max Wallace from the Accelerate Brain Cancer Cure (ABC<sup>2</sup>), Washington, D.C., Al Musella from the Musella Foundation, Hewlett, NY, and Chas Haynes from the Collaborative Ependymoma Research Network, Dayton, OH.

## References

1. Rosen BR, Belliveau JW, Vevea JM, Brady TJ. Perfusion imaging with NMR contrast agents. *Magn Reson Med*. 1990; 14(2):249-265.
2. Belliveau JW, Kennedy DN, Jr., McKinstry RC, et al. Functional mapping of the human visual cortex by magnetic resonance imaging. *Science*. 1991; 254(5032):716-719.
3. Aronen HJ, Gazit IE, Louis DN, et al. Cerebral blood volume maps of gliomas: comparison with tumor grade and histologic findings. *Radiology*. 1994; 191(1):41-51.
4. Maeda M, Itoh S, Kimura H, et al. Tumor vascularity in the brain: evaluation with dynamic susceptibility-contrast MR imaging. *Radiology*. 1993; 189(1):233-238.
5. Donahue KM, Krouwer HG, Rand SD, et al. Utility of simultaneously acquired gradient-echo and spin-echo cerebral blood volume and morphology maps in brain tumor patients. *Magn Reson Med*. 2000; 43(6):845-853.
6. Aronen HJ, Pardo FS, Kennedy DN, et al. High microvascular blood volume is associated with high glucose uptake and tumor angiogenesis in human gliomas. *Clin Cancer Res*. 2000; 6(6):2189-2200.
7. Sugahara T, Korogi Y, Kochi M, Ushio Y, Takahashi M. Perfusion-sensitive MR imaging of gliomas: comparison between gradient-echo and spin-echo echo-planar imaging techniques. *AJNR Am J Neuroradiol*. 2001; 22(7):1306-1315.
8. Boxerman JL, Schmainda KM, Weisskoff RM. Relative cerebral blood volume maps corrected for contrast agent extravasation significantly correlate with glioma tumor grade, whereas uncorrected maps do not. *AJNR Am J Neuroradiol*. 2006; 27(4):859-867.



9. Law M, Oh S, Babb JS, et al. Low-grade gliomas: dynamic susceptibility-weighted contrast-enhanced perfusion MR imaging--prediction of patient clinical response. *Radiology*. 2006; 238(2):658-667.
10. Jiang Z, Le Bas JF, Grand S, et al. Prognostic value of perfusion MR imaging in patients with oligodendroglioma: A survival study. *J Neuroradiol*. 2011; 38(1):53-61.
11. Hipp SJ, Steffen-Smith E, Hammoud D, Shih JH, Bent R, Warren KE. Predicting outcome of children with diffuse intrinsic pontine gliomas using multiparametric imaging. *Neuro-oncology*. 2011; 13(8):904-909.
12. Bonekamp D, Deike K, Wiestler B, et al. Association of overall survival in patients with newly diagnosed glioblastoma with contrast-enhanced perfusion MRI: Comparison of intraindividually matched T1 - and T2 (\*) -based bolus techniques. *Journal of magnetic resonance imaging : JMRI*. 2015; 42(1):87-96.
13. Jabehdar Maralani P, Melhem ER, Wang S, et al. Association of dynamic susceptibility contrast enhanced MR Perfusion parameters with prognosis in elderly patients with glioblastomas. *Eur Radiol*. 2015; 25(9):2738-2744.
14. Barajas RF, Jr., Chang JS, Segal MR, et al. Differentiation of recurrent glioblastoma multiforme from radiation necrosis after external beam radiation therapy with dynamic susceptibility-weighted contrast-enhanced perfusion MR imaging. *Radiology*. 2009; 253(2):486-496.
15. Hu LS, Baxter LC, Smith KA, et al. Relative cerebral blood volume values to differentiate high-grade glioma recurrence from posttreatment radiation effect: direct correlation between image-guided tissue histopathology and localized dynamic

susceptibility-weighted contrast-enhanced perfusion MR imaging measurements. *AJNR Am J Neuroradiol*. 2009; 30(3):552-558.

16. Gasparetto EL, Pawlak MA, Patel SH, et al. Posttreatment recurrence of malignant brain neoplasm: accuracy of relative cerebral blood volume fraction in discriminating low from high malignant histologic volume fraction. *Radiology*. 2009; 250(3):887-896.
17. Kim HS, Goh MJ, Kim N, Choi CG, Kim SJ, Kim JH. Which combination of MR imaging modalities is best for predicting recurrent glioblastoma? Study of diagnostic accuracy and reproducibility. *Radiology*. 2014; 273(3):831-843.
18. Hu LS, Eschbacher JM, Heiserman JE, et al. Reevaluating the imaging definition of tumor progression: perfusion MRI quantifies recurrent glioblastoma tumor fraction, pseudoprogression, and radiation necrosis to predict survival. *Neuro-oncology*. 2012; 14(7):919-930.
19. Young RJ, Gupta A, Shah AD, et al. MRI perfusion in determining pseudoprogression in patients with glioblastoma. *Clin Imaging*. 2013; 37(1):41-49.
20. Schmainda KM, Prah M, Connelly J, et al. Dynamic-susceptibility contrast agent MRI measures of relative cerebral blood volume predict response to bevacizumab in recurrent high-grade glioma. *Neuro-oncology*. 2014; 16(6):880-888.
21. Leu K, Enzmann DR, Woodworth DC, et al. Hypervascular tumor volume estimated by comparison to a large-scale cerebral blood volume radiographic atlas predicts survival in recurrent glioblastoma treated with bevacizumab. *Cancer Imaging*. 2014; 14:31.

22. Aquino D, Di Stefano AL, Scotti A, et al. Parametric response maps of perfusion MRI may identify recurrent glioblastomas responsive to bevacizumab and irinotecan. *PLoS One*. 2014; 9(3):e90535.
23. Schmainda KM, Zhang Z, Prah M, et al. Dynamic Susceptibility Contrast MRI Measures of Relative Cerebral Blood Volume as a Prognostic Marker for Overall Survival in Recurrent Glioblastoma: Results from the ACRIN 6677/RTOG 0625 Multi-Center Trial. *Neuro-oncology*. 2015; 17(8):1148-1156.
24. Kickingeder P, Wiestler B, Burth S, et al. Relative cerebral blood volume is a potential predictive imaging biomarker of bevacizumab efficacy in recurrent glioblastoma. *Neuro-oncology*. 2015; 17(8):1139-1147.
25. Harris RJ, Cloughesy TF, Hardy AJ, et al. MRI perfusion measurements calculated using advanced deconvolution techniques predict survival in recurrent glioblastoma treated with bevacizumab. *Journal of neuro-oncology*. 2015; 122(3):497-505.
26. Geer CP, Simonds J, Anvery A, et al. Does MR perfusion imaging impact management decisions for patients with brain tumors? A prospective study. *AJNR Am J Neuroradiol*. 2012; 33(3):556-562.
27. Willats L, Calamante F. The 39 steps: evading error and deciphering the secrets for accurate dynamic susceptibility contrast MRI. *NMR Biomed*. 2013; 26(8):913-931.
28. Semmineh NB, Xu J, Skinner JT, et al. Assessing tumor cytoarchitecture using multiecho DSC-MRI derived measures of the transverse relaxivity at tracer equilibrium (TRATE). *Magn Reson Med*. 2015; 74(3):772-784.

29. Stokes AM, Skinner JT, Yankeelov T, Quarles CC. Assessment of a simplified spin and gradient echo (sSAGE) approach for human brain tumor perfusion imaging. *Magn Reson Imaging*. 2016; 34(9):1248-1255.
30. Ellingson BM, Bendszus M, Boxerman J, et al. Consensus recommendations for a standardized Brain Tumor Imaging Protocol in clinical trials. *Neuro-oncology*. 2015; 17(9):1188-1198.
31. Meier P, Zierler KL. On the theory of the indicator-dilution method for measurement of blood flow and volume. *J Appl Physiol*. 1954; 6(12):731-744.
32. Villringer A, Rosen BR, Belliveau JW, et al. Dynamic imaging with lanthanide chelates in normal brain: contrast due to magnetic susceptibility effects. *Magn Reson Med*. 1988; 6(2):164-174.
33. Rempp KA, Brix G, Wenz F, Becker CR, Guckel F, Lorenz WJ. Quantification of regional cerebral blood flow and volume with dynamic susceptibility contrast-enhanced MR imaging. *Radiology*. 1994; 193(3):637-641.
34. Bedekar D, Jensen T, Schmainda KM. Standardization of relative cerebral blood volume (rCBV) image maps for ease of both inter- and inpatient comparisons. *Magn Reson Med*. 2010; 64(3):907-913.
35. Ellingson BM, Zaw T, Cloughesy TF, et al. Comparison between intensity normalization techniques for dynamic susceptibility contrast (DSC)-MRI estimates of cerebral blood volume (CBV) in human gliomas. *Journal of magnetic resonance imaging : JMRI*. 2012; 35(6):1472-1477.

36. Boxerman JL, Hamberg LM, Rosen BR, Weisskoff RM. MR contrast due to intravascular magnetic susceptibility perturbations. *Magn Reson Med*. 1995; 34(4):555-566.
37. Fisel CR, Ackerman JL, Buxton RB, et al. MR contrast due to microscopically heterogeneous magnetic susceptibility: numerical simulations and applications to cerebral physiology. *Magn Reson Med*. 1991; 17(2):336-347.
38. Schmiedeskamp H, Straka M, Newbould RD, et al. Combined spin- and gradient-echo perfusion-weighted imaging. *Magn Reson Med*. 2012; 68(1):30-40.
39. Zama A, Tamura M, Inoue HK. Three-dimensional observations on microvascular growth in rat glioma using a vascular casting method. *J Cancer Res Clin Oncol*. 1991; 117(5):396-402.
40. Badruddoja MA, Krouwer HG, Rand SD, Rebro KJ, Pathak AP, Schmainda KM. Antiangiogenic effects of dexamethasone in 9L gliosarcoma assessed by MRI cerebral blood volume maps. *Neuro-oncology*. 2003; 5(4):235-243.
41. Weisskoff RM, Zuo CS, Boxerman JL, Rosen BR. Microscopic susceptibility variation and transverse relaxation: theory and experiment. *Magn Reson Med*. 1994; 31(6):601-610.
42. Paulson ES, Schmainda KM. Comparison of dynamic susceptibility-weighted contrast-enhanced MR methods: recommendations for measuring relative cerebral blood volume in brain tumors. *Radiology*. 2008; 249(2):601-613.
43. Quarles CC, Gochberg DF, Gore JC, Yankeelov TE. A theoretical framework to model DSC-MRI data acquired in the presence of contrast agent extravasation. *Phys Med Biol*. 2009; 54(19):5749-5766.

44. Cha S, Knopp EA, Johnson G, Wetzel SG, Litt AW, Zagzag D. Intracranial mass lesions: dynamic contrast-enhanced susceptibility-weighted echo-planar perfusion MR imaging. *Radiology*. 2002; 223(1):11-29.
45. Schmainda KM, Rand SD, Joseph AM, et al. Characterization of a first-pass gradient-echo spin-echo method to predict brain tumor grade and angiogenesis. *AJNR Am J Neuroradiol*. 2004; 25(9):1524-1532.
46. Quarles CC, Ward BD, Schmainda KM. Improving the reliability of obtaining tumor hemodynamic parameters in the presence of contrast agent extravasation. *Magn Reson Med*. 2005; 53(6):1307-1316.
47. Leu K, Boxerman JL, Lai A, et al. Bidirectional Contrast agent leakage correction of dynamic susceptibility contrast (DSC)-MRI improves cerebral blood volume estimation and survival prediction in recurrent glioblastoma treated with bevacizumab. *Journal of magnetic resonance imaging : JMRI*. 2016; 44(5):1229-1237.
48. Paulson ES, Prah DE, Schmainda KM. Spiral Perfusion Imaging With Consecutive Echoes (SPICE) for the Simultaneous Mapping of DSC- and DCE-MRI Parameters in Brain Tumor Patients: Theory and Initial Feasibility. *Tomography*. 2016; 2(4):295-307.
49. Vonken EP, van Osch MJ, Bakker CJ, Viergever MA. Simultaneous quantitative cerebral perfusion and Gd-DTPA extravasation measurement with dual-echo dynamic susceptibility contrast MRI. *Magn Reson Med*. 2000; 43(6):820-827.
50. Gahramanov S, Muldoon LL, Li X, Neuwelt EA. Improved perfusion MR imaging assessment of intracerebral tumor blood volume and antiangiogenic therapy efficacy in a rat model with ferumoxytol. *Radiology*. 2011; 261(3):796-804.

51. Horvath A, Varallyay CG, Schwartz D, et al. Quantitative comparison of delayed ferumoxytol T1 enhancement with immediate gadoteridol enhancement in high grade gliomas. *Magn Reson Med*. 2018; 80(1):224-230.
52. Hu LS, Baxter LC, Pinnaduwege DS, et al. Optimized preload leakage-correction methods to improve the diagnostic accuracy of dynamic susceptibility-weighted contrast-enhanced perfusion MR imaging in posttreatment gliomas. *AJNR Am J Neuroradiol*. 2010; 31(1):40-48.
53. Weisskoff RM, Boxerman JL, Sorensen AG, Kulke SM, Campbell TA, Rosen BR. Simultaneous blood volume and permeability mapping using a single Gd-based contrast injection. Paper presented at: Society of Magnetic Resonance in Medicine, 2nd Annual Meeting 1994; San Francisco, CA.
54. Bjornerud A, Sorensen AG, Mouridsen K, Emblem KE. T1- and T2\*-dominant extravasation correction in DSC-MRI: part I--theoretical considerations and implications for assessment of tumor hemodynamic properties. *J Cereb Blood Flow Metab*. 2011; 31(10):2041-2053.
55. Leu K, Boxerman JL, Cloughesy TF, et al. Improved Leakage Correction for Single-Echo Dynamic Susceptibility Contrast Perfusion MRI Estimates of Relative Cerebral Blood Volume in High-Grade Gliomas by Accounting for Bidirectional Contrast Agent Exchange. *AJNR Am J Neuroradiol*. 2016; 37(8):1440-1446.
56. Welker K, Boxerman J, Kalnin A, et al. ASFNR recommendations for clinical performance of MR dynamic susceptibility contrast perfusion imaging of the brain. *AJNR Am J Neuroradiol*. 2015; 36(6):E41-51.

57. Boxerman JL, Prah DE, Paulson ES, Machan JT, Bedekar D, Schmainda KM. The Role of preload and leakage correction in gadolinium-based cerebral blood volume estimation determined by comparison with MION as a criterion standard. *AJNR Am J Neuroradiol*. 2012; 33(6):1081-1087.
58. Hu LS, Eschbacher JM, Dueck AC, et al. Correlations between perfusion MR imaging cerebral blood volume, microvessel quantification, and clinical outcome using stereotactic analysis in recurrent high-grade glioma. *AJNR Am J Neuroradiol*. 2012; 33(1):69-76.
59. Prah MA, Al-Gizawiy MM, Mueller WM, et al. Spatial discrimination of glioblastoma and treatment effect with histologically-validated perfusion and diffusion magnetic resonance imaging metrics. *Journal of neuro-oncology*. 2018; 136(1):13-21.
60. Prah MA, Stufflebeam SM, Paulson ES, et al. Repeatability of Standardized and Normalized Relative CBV in Patients with Newly Diagnosed Glioblastoma. *AJNR Am J Neuroradiol*. 2015; 36(9):1654-1661.
61. Gerstner ER, Zhang Z, Fink JR, et al. ACRIN 6684: Assessment of Tumor Hypoxia in Newly Diagnosed Glioblastoma Using 18F-FMISO PET and MRI. *Clin Cancer Res*. 2016; 22(20):5079-5086.
62. Hu LS, Kelm Z, Korfiatis P, et al. Impact of Software Modeling on the Accuracy of Perfusion MRI in Glioma. *AJNR Am J Neuroradiol*. 2015; 36(12):2242-2249.
63. Bell LC, Semmineh N, An H, et al. Evaluating Multisite rCBV Consistency from DSC-MRI Imaging Protocols and Postprocessing Software Across the NCI Quantitative Imaging Network Sites Using a Digital Reference Object (DRO). *Tomography*. 2019; 5(1):110-117.



64. Schmainda KM, Prah MA, Rand SD, et al. Multisite Concordance of DSC-MRI Analysis for Brain Tumors: Results of a National Cancer Institute Quantitative Imaging Network Collaborative Project. *AJNR Am J Neuroradiol*. 2018; 39(6):1008-1016.
65. Semmineh NB, Stokes AM, Bell LC, Boxerman JL, Quarles CC. A Population-Based Digital Reference Object (DRO) for Optimizing Dynamic Susceptibility Contrast (DSC)-MRI Methods for Clinical Trials. *Tomography*. 2017; 3(1):41-49.
66. Semmineh NB, Bell LC, Stokes AM, Hu LS, Boxerman JL, Quarles CC. Optimization of Acquisition and Analysis Methods for Clinical Dynamic Susceptibility Contrast (DSC) MRI Using a Population-based Digital Reference Object. *AJNR Am J Neuroradiol*. 2018; 39(11):1981-1988.
67. Boxerman JL, Rosen BR, Weisskoff RM. Signal-to-noise analysis of cerebral blood volume maps from dynamic NMR imaging studies. *Journal of magnetic resonance imaging : JMRI*. 1997; 7(3):528-537.
68. Thilmann O, Larsson EM, Bjorkman-Burtscher IM, Stahlberg F, Wirestam R. Effects of echo time variation on perfusion assessment using dynamic susceptibility contrast MR imaging at 3 tesla. *Magn Reson Imaging*. 2004; 22(7):929-935.
69. Knutsson L, Stahlberg F, Wirestam R. Aspects on the accuracy of cerebral perfusion parameters obtained by dynamic susceptibility contrast MRI: a simulation study. *Magn Reson Imaging*. 2004; 22(6):789-798.
70. Smith MR, Lu H, Frayne R. Signal-to-noise ratio effects in quantitative cerebral perfusion using dynamic susceptibility contrast agents. *Magn Reson Med*. 2003; 49(1):122-128.

71. Barajas RF, Jr., Hodgson JG, Chang JS, et al. Glioblastoma multiforme regional genetic and cellular expression patterns: influence on anatomic and physiologic MR imaging. *Radiology*. 2010; 254(2):564-576.
72. Das S, Marsden PA. Angiogenesis in glioblastoma. *The New England journal of medicine*. 2013; 369(16):1561-1563.
73. Brandsma D, van den Bent MJ. Pseudoprogression and pseudoresponse in the treatment of gliomas. *Current opinion in neurology*. 2009; 22(6):633-638.
74. Wen PY, Macdonald DR, Reardon DA, et al. Updated response assessment criteria for high-grade gliomas: response assessment in neuro-oncology working group. *J Clin Oncol*. 2010; 28(11):1963-1972.
75. Prager AJ, Martinez N, Beal K, Omuro A, Zhang Z, Young RJ. Diffusion and perfusion MRI to differentiate treatment-related changes including pseudoprogression from recurrent tumors in high-grade gliomas with histopathologic evidence. *AJNR Am J Neuroradiol*. 2015; 36(5):877-885.
76. Mangla R, Singh G, Ziegelitz D, et al. Changes in relative cerebral blood volume 1 month after radiation-temozolomide therapy can help predict overall survival in patients with glioblastoma. *Radiology*. 2010; 256(2):575-584.
77. Kong DS, Kim ST, Kim EH, et al. Diagnostic dilemma of pseudoprogression in the treatment of newly diagnosed glioblastomas: the role of assessing relative cerebral blood flow volume and oxygen-6-methylguanine-DNA methyltransferase promoter methylation status. *AJNR Am J Neuroradiol*. 2011; 32(2):382-387.

- 78.** Boxerman JL, Ellingson BM, Jeyapalan S, et al. Longitudinal DSC-MRI for Distinguishing Tumor Recurrence From Pseudoprogression in Patients With a High-grade Glioma. *Am J Clin Oncol*. 2017; 40(3):228-234.
- 79.** Patel P, Baradaran H, Delgado D, et al. MR perfusion-weighted imaging in the evaluation of high-grade gliomas after treatment: a systematic review and meta-analysis. *Neuro-oncology*. 2017; 19(1):118-127.
- 80.** Ostergaard L, Weisskoff RM, Chesler DA, Gyldensted C, Rosen BR. High resolution measurement of cerebral blood flow using intravascular tracer bolus passages. Part I: Mathematical approach and statistical analysis. *Magn Reson Med*. 1996; 36(5):715-725.
- 81.** Leu K, Boxerman JL, Ellingson BM. Effects of MRI Protocol Parameters, Preload Injection Dose, Fractionation Strategies, and Leakage Correction Algorithms on the Fidelity of Dynamic-Susceptibility Contrast MRI Estimates of Relative Cerebral Blood Volume in Gliomas. *AJNR Am J Neuroradiol*. 2017; 38(3):478-484.
- 82.** Schmainda KM, Prah MA, Hu LS, et al. Moving Toward a Consensus DSC-MRI Protocol: Validation of a Low-Flip Angle Single-Dose Option as a Reference Standard for Brain Tumors. *AJNR Am J Neuroradiol*. 2019.

## Figure Captions

### Figure 1.

DSC-MRI methodology in the literature varies greatly, as seen in the subgroup meta-analysis by Patel et al. of studies using mean lesion rCBV for recurrent high-grade tumor vs. treatment effect. These studies used a wide range of DSC-MRI parameters including TE, FA, preload dose and post-processing leakage correction (PPLC). (Adapted from Ref. [79].)

### Figure 2.

Possible BTIP-compliant DSC-MRI preload + bolus dose paradigms. Either a single total dose must be split between preload and DSC-MRI before post-GBCA imaging, or a full dose preload must be given with DSC-MRI after post-contrast imaging.

### Figure 3.

Computational approach for determining optimal BTIP-compliant DSC-MRI parameters using simulated DSC-MRI signal with GBCA leakage: heat maps of CBV error versus theoretical CBV without leakage for different combinations of acquisition parameters. Schemes with particularly high fidelity at 3T include 60° FA with full-dose preload and bolus (asterisk with dashed box) and low FA without preload (asterisk with solid box). (Adapted from Ref. [81].)

### Figure 4.

Computational approach for determining optimal BTIP-compliant DSC-MRI parameters using a digital reference object matched to glioblastoma training data: performance comparison for intermediate and low flip angle schemes. For double-dose contrast with

full-dose preload, both schemes have excellent accuracy and precision at 1.5T and 3T. For single-dose contrast without preload, intermediate FA performs poorly but low FA maintains excellent performance, even at 1.5T. For each dosing scheme, low FA had equal or better performance than intermediate FA. CCC = Concordance correlation coefficient (accuracy); CV = coefficient of variation (precision). (Adapted from Ref. [66].)

**Figure 5.**

- A) DRO-based simulations demonstrate that even without preload, low FA (30°) acquisitions give very accurate CBV (along the line of unity) with much less bias compared to intermediate FA (60°) acquisitions, even at 1.5T. (Adapted from Ref. [66].)
- B) Excellent CBV agreement has been observed in vivo at 3T for “0+1” and “1+1” dosing schemes, according to Lin’s concordance correlation (CCC).

# **Consensus Recommendations for a Dynamic Susceptibility Contrast MRI Protocol for Use in High-Grade Gliomas**

Jerrold L. Boxerman<sup>1,¥,Ω,£</sup>, Chad C. Quarles<sup>2</sup>, Leland S. Hu<sup>24,◇,Ω</sup>,  
Bradley J. Erickson<sup>3,◇,æ,Ω</sup>, Elizabeth R. Gerstner<sup>4,†</sup>, Marion Smits<sup>5,β</sup>,  
Timothy J. Kaufmann<sup>3,◇</sup>, Daniel P. Barboriak<sup>6,¥,æ,Ω</sup>, Raymond H. Huang<sup>8,9</sup>,  
Wolfgang Wick<sup>10,β</sup>, Michael Weller<sup>11,β</sup>, Evanthia Galanis<sup>12,◇</sup>,  
Jayashree Kalpathy-Cramer<sup>13</sup>, Lalitha Shankar<sup>14</sup>, Paula Jacobs<sup>14</sup>, Caroline Chung<sup>15,◇</sup>,  
Martin J. van den Bent<sup>16,β</sup>, Susan Chang<sup>17</sup>, W.K. Al Yung<sup>18</sup>, Timothy F. Cloughesy<sup>19,20</sup>,  
Patrick Y. Wen<sup>9,†</sup>, Mark R. Gilbert<sup>21,¢</sup>, Bruce R. Rosen<sup>13</sup>,  
Benjamin M. Ellingson<sup>19,22,†,§,¥,æ,Ω</sup>, and Kathleen M. Schmainda<sup>23,¥</sup>

and the Jumpstarting Brain Tumor Drug Development Coalition  
Imaging Standardization Steering Committee

Affiliations:

<sup>1</sup> Department of Diagnostic Imaging, Warren Alpert Medical School, Brown University, Providence, RI

<sup>2</sup> Department of Neuroimaging Research & Barrow Neuroimaging Innovation Center, Barrow Neurological Institute, Phoenix, AZ

<sup>3</sup> Department of Radiology, Mayo Clinic, Rochester, MN

<sup>4</sup> Department of Neurology, Massachusetts General Hospital, Harvard Medical School, Boston, MA

<sup>5</sup> Department of Radiology and Nuclear Medicine, Erasmus MC – University Medical Center Rotterdam, Rotterdam, Netherlands

<sup>6</sup> Department of Radiology, Duke University School of Medicine, Durham, NC

<sup>8</sup> Department of Radiology, Brigham and Women's Hospital, Boston, MA

<sup>9</sup> Center for Neuro-Oncology, Dana-Farber/Brigham and Women's Cancer Center, Harvard Medical School, Boston, MA

<sup>10</sup> Department of Neurooncology, National Center of Tumor Disease, University Clinic Heidelberg, Heidelberg, Germany

<sup>11</sup> Department of Neurology, University Hospital and University of Zurich, Zurich, Switzerland

<sup>12</sup> Division of Medical Oncology, Department of Oncology, Mayo Clinic, Rochester, MN

<sup>13</sup> Martinos Center for Biomedical Imaging, Massachusetts General Hospital and Harvard Medical School, Boston, MA

<sup>14</sup> Division of Cancer Treatment and Diagnosis, National Cancer Institute (NCI), Bethesda, MD

<sup>15</sup> Department of Radiation Oncology, The University of Texas MD Anderson Cancer Center, Houston, TX

<sup>16</sup> Department of Neuro-Oncology, Erasmus MC Cancer Institute, Rotterdam, Netherlands

<sup>17</sup> Department of Neurological Surgery, University of California – San Francisco, San Francisco, CA

<sup>18</sup> Department of Neuro-Oncology, Division of Cancer Medicine, The University of Texas MD Anderson Cancer Center, Houston, TX

<sup>19</sup> UCLA Neuro-Oncology Program & UCLA Brain Tumor Imaging Laboratory (BTIL), David Geffen School of Medicine, University of California – Los Angeles, Los Angeles, CA

<sup>20</sup> Department of Neurology, David Geffen School of Medicine, University of California – Los Angeles, Los Angeles, CA

<sup>21</sup> Neuro-Oncology Branch, National Cancer Institute (NCI), Bethesda, MD

<sup>22</sup> Departments of Radiological Sciences, Psychiatry, and Biobehavioral Sciences, David Geffen School of Medicine, University of California – Los Angeles, Los Angeles, CA

<sup>23</sup> Department of Biophysics, Medical College of Wisconsin, Milwaukee, WI

<sup>24</sup> Department of Radiology, Mayo Clinic, Arizona

Additional Affiliations:

† Representative of the Adult Brain Tumor Consortium (ABTC)

§ Representative of the Ivy Consortium for Early Phase Clinical Trials



¥ Representative of the Eastern Cooperative Oncology Group – American College of Radiology Imaging Network (ECOG-ACRIN) Cancer Research Group

ß Representative of the European Organization for Research and Treatment of Cancer (EORTC)

◇ Representative of the Alliance for Clinical Trials in Oncology

æ Representative of the RSNA Quantitative Imaging Biomarker Alliance (QIBA)

Ω Representative of the American Society of Neuroradiology (ASNR)

£ Representative of the American Society of Functional Neuroradiology (ASFNR)

¢ Representative of the Radiation Therapy Oncology Group (RTOG)

**Corresponding author:** Jerrold L. Boxerman, MD, PhD

Rhode Island Hospital, Department of Diagnostic Imaging

593 Eddy Street

Providence, RI 02903

(401) 444-5184 (Phone)

(401) 444-5017 (Fax)

*jboxerman@lifespan.org*

## Abstract

Despite the widespread clinical use of dynamic susceptibility contrast (DSC) MRI, DSC-MRI methodology has not been standardized, hindering its utilization for response assessment in multi-center trials. Recently, the DSC-MRI Standardization Subcommittee of the Jumpstarting Brain Tumor Drug Development Coalition issued an updated consensus DSC-MRI protocol compatible with BTIP, the standardized brain tumor imaging protocol for high-grade gliomas that is increasingly used in the clinical setting and is the default MRI protocol for the National Clinical Trials Network. After reviewing the basis for controversy over DSC-MRI protocols, this manuscript provides evidence-based best practices for clinical DSC-MRI as determined by the Committee, including pulse sequence (gradient echo vs. spin echo), BTIP-compliant contrast agent dosing (preload and bolus), flip angle (FA), echo time (TE), and post-processing leakage correction. In summary, full-dose preload, full-dose bolus dosing using intermediate ( $60^\circ$ ) FA and field strength-dependent TE (40-50ms at 1.5T, 20-35ms at 3T) provides overall best accuracy and precision for cerebral blood volume estimates. When single-dose contrast agent usage is desired, no-preload, full-dose bolus dosing using low FA ( $30^\circ$ ) and field strength-dependent TE provides excellent performance, with reduced contrast agent usage and elimination of potential systematic errors introduced by variations in preload dose and incubation time.

**Keywords:** DSC-MRI; cerebral blood volume; high-grade glioma; clinical trial; consensus protocol

## Introduction

In 1990, Rosen et al. demonstrated transiently decreased brain signal intensity after bolus administration of gadolinium-based contrast agent (GBCA).<sup>1</sup> The signal intensity-time curve could be converted into a concentration-time curve, enabling voxel-wise computation of cerebral blood volume (CBV). This technique, now widely known as dynamic susceptibility contrast (DSC) MRI, uses the magnetic susceptibility properties of paramagnetic contrast agents (gadolinium chelates or superparamagnetic nanoparticles) and T2 or T2\*-weighted acquisitions. DSC-MRI was used to perform the first “functional” MRI experiments of task-induced brain activation,<sup>2</sup> and produce the first MRI-based CBV maps of gliomas.<sup>3</sup>

Since these beginnings, studies have shown that DSC-MRI may be more useful than standard MRI at predicting treatment-naïve glioma grade<sup>3-8</sup> and survival,<sup>9-13</sup> distinguishing post-treatment pseudoprogression and radiation necrosis from recurrent tumor,<sup>14-17</sup> and predicting response to anti-angiogenic therapy.<sup>18-25</sup> Use of DSC-MRI has consequently exploded over the past few decades, particularly in neuro-oncology. Geer et al. found that the addition of DSC-MRI increased the confidence of neuroradiologists and treating physicians in their assessment of tumor status in 40% and 56% of cases, respectively, with treatment modification in 8.5% of patients,<sup>26</sup> highlighting the potential clinical impact of DSC-MRI. Despite this and other evidence for clinical impact on the management of brain tumor patients, technical aspects of DSC-MRI have not been standardized, which has hindered its widespread adoption and utilization for assessment of treatment response in multi-center therapeutic trials.

There are multiple protocol decisions for DSC-MRI that influence its practical implementation and the accuracy and precision of CBV measurement.<sup>27</sup> These include gradient echo (GRE) versus spin echo (SE) pulse sequence; contrast agent dosing, including preload and bolus; image acquisition parameters, including flip angle (FA), echo time (TE), temporal resolution (TR) and number of baseline and post-bolus data points; and post-processing techniques, including GBCA leakage correction. After reviewing the basis for controversy over DSC-MRI protocol, this manuscript provides *evidence-based best practices for clinical DSC-MRI*, emphasizing our favored choices for these protocol decisions. The *evidence* comes from DSC-MRI theory, computer modeling and simulation of DSC-MRI signal acquisition and post-processing, in vivo stereotactic tissue correlation, and single-institution and multi-site clinical trial data. Because a primary goal for harmonizing DSC-MRI methodology is the facilitation of its widespread adoption and the collation of results from multi-site trials, for *best clinical practice* we emphasize CBV *accuracy* and *precision* in neuro-oncology applications, including treatment response assessment of high-grade gliomas in clinical trials of novel therapeutics. Although advanced DSC-MRI methods including multi-echo approaches may measure additional features of tumor pathophysiology (including vessel caliber, vascular permeability, tumor cell size and cytoarchitecture),<sup>28,29</sup> our recommendations focus on CBV measurement using single TE, GRE echo planar imaging and GBCA-based DSC-MRI, which is the most common methodology in practice and is concordant with other widely adopted brain tumor imaging protocols.<sup>30</sup>

## A Brief Overview of DSC-MRI

DSC-MRI is based upon classical indicator dilution theory used by physiologists to quantitate hemodynamics of whole-organ systems from known quantities of injected non-diffusible tracers such as dyes and radiotracers, and measurement of output tracer concentration.<sup>31</sup> DSC-MRI applies this methodology to the brain, using exogenous paramagnetic GBCA as the “tracer”. DSC-MRI is a “bolus tracking” technique that rapidly acquires GRE or SE echo planar images before (baseline), during (bolus), and after (tail) first-pass transit through the brain of GBCA that transiently alters the acquired signal intensity.<sup>32</sup> Voxel-wise changes in relative contrast agent concentration are determined by converting the signal intensity-time curves into change in relaxation rate-time curves, assuming that transient signal loss is due solely to magnetic susceptibility effects resulting from the injected GBCA and the subsequent changes in  $T2^*$  (GRE) or  $T2$  (SE) relaxation rate ( $\Delta R2^*$  and  $\Delta R2$ , respectively, and herein referred to collectively as  $\Delta R2^*$  unless otherwise specified). Because  $\Delta R2^*$  is assumed to be directly proportional to tissue GBCA concentration, with GBCA confined to the vasculature, the  $\Delta R2^*$ -time curves are processed using tracer kinetic modeling and indicator dilution theory to estimate cerebral hemodynamic parameters such as CBV, cerebral blood flow (CBF), and mean transit time (MTT).<sup>1</sup> Absolute CBV can theoretically be determined from the area under the  $\Delta R2^*$ -time curve normalized to the integrated arterial input function (AIF).<sup>33</sup> Most often, to avoid the well-known difficulties of accurately determining the AIF, relative CBV (rCBV) is estimated from the area under the  $\Delta R2^*$ -time curve alone giving a CBV value that has meaning relative to other parts of the brain. For comparison across time and patients, rCBV may be normalized to rCBV in normal-appearing white matter, yielding the most

common DSC-MRI metric for evaluating brain tumors, normalized rCBV (nRCBV). Alternative methods precluding the need to normalize rCBV to reference brain include standardization and Gaussian normalization.<sup>34,35</sup>

## **Basic Contrast Mechanism for DSC-MRI**

The DSC-MRI contrast mechanism is based upon compartmentalization of paramagnetic GBCA that establishes magnetic susceptibility difference between the intra- and extra-vascular space, creating magnetic field gradients.<sup>32</sup> Protons lose phase coherence as they diffuse through the transient, spatially varying gradients, yielding signal attenuation dependent upon physiological factors, including vessel or compartment size and proton diffusion rate, and experimental factors, including pulse sequence parameters and contrast agent concentration.<sup>36</sup> Although this behavior can be solved analytically for limited regimes, this phenomenon has been most generally studied using Monte Carlo numerical methods that quantify the relationship between change in relaxation rate and the physiological and experimental parameters.<sup>36,37</sup> These simulations yield the vessel size-dependence relationships for GRE ( $\Delta R2^*$ ) and SE ( $\Delta R2$ ) change in relaxation rate, with  $\Delta R2^*$  plateauing for large diameter vessels, and  $\Delta R2$  peaking for capillary-sized vessels (e.g., Figure 1 in Ref. [36]). These relationships are qualitatively independent of vessel geometry.

## **Gradient-echo versus Spin-echo Acquisitions**

The vessel size-dependence relationships have clinical implications. Because  $\Delta R2$  peaks for microvessels, SE DSC-MRI is advantageous in stroke imaging aimed at

identifying capillary-level perfusion deficits,<sup>38</sup> with reduced blooming artifact in cortex around sulcal vessels. GRE DSC-MRI is sensitive to the larger, disorganized vessels that characterize high-grade gliomas,<sup>39,40</sup> with obvious application to tumor imaging. For given contrast agent concentration, field strength, and imaging parameters,  $\Delta R2^*$  exceeds  $\Delta R2$  for all vessel sizes, with larger corresponding signal loss.<sup>36</sup> Therefore, GRE-derived CBV maps have higher inherent SNR and sensitivity than SE CBV maps, and can provide greater signal changes for equal GBCA dose, or equivalent signal changes with lower GBCA dose, compared to those derived with SE DSC-MRI.

In order for DSC-MRI to accurately measure cerebral hemodynamics, there must be a linear relationship between change in relaxation rate and GBCA concentration. From basic susceptibility contrast principles, change in relaxation rate is directly proportional to GBCA concentration only where the  $\Delta R2$  or  $\Delta R2^*$  versus vessel size curves are “plateaued”.<sup>41</sup> This plateau occurs over a much broader range of vessel sizes for GRE ( $\Delta R2^*$ ) compared to SE ( $\Delta R2$ ) DSC-MRI, and so GRE CBV estimates are inherently more accurate than SE CBV estimates. Similarly, the  $x$ -axis of the size-dependence curves actually scales as  $R^2/D$ , where  $R$  is the vessel size and  $D$  is the proton diffusion rate.<sup>41</sup> Therefore, decreasing  $D$  (restricted diffusion) has the same effect as increasing vessel size (moving to the right on the change in relaxation rate versus vessel size graphs). While increasing vessel diameter or decreasing diffusion can result in either increased or decreased  $\Delta R2$ ,  $\Delta R2^*$  will be much less affected because of the plateau in the  $\Delta R2^*$ -size curve. Therefore, in tumors with heterogeneous proton diffusion and abnormal vascular morphology, hyperintensity on CBV maps is more likely to reflect truly elevated blood volume for GRE acquisitions versus greater uncertainty for SE acquisitions.

For these reasons – sensitivity to larger, disorganized microvessels seen in higher-grade tumors; greater signal changes for a given contrast agent dose; greater inherent accuracy of CBV estimates; and decreased sensitivity to changes in proton diffusion – GRE DSC-MRI is recommended for neuro-oncology applications. Thus, moving forward, we will only refer to T2\* changes that occur with GRE DSC-MRI.

## **Consequences of Contrast Agent Extravasation**

Another requirement for DSC-MRI to mimic tracer kinetics is that contrast agent must remain intravascular, which is violated for GBCAs in high-grade gliomas (HGG) with blood-brain barrier (BBB) disruption and avid contrast enhancement. GBCA extravasation results in T1 shortening, opposing the susceptibility contrast induced T2\* relaxation rate change from intravascular GBCA that forms the basis for CBV estimation. Because GBCA is excluded from cells, GBCA extravasation establishes a magnetic susceptibility gradient not only between the intra- and extra-vascular spaces, but also between the intra- and extra-cellular spaces when sufficient GBCA distributes throughout the extravascular-extracellular space, potentially exaggerating T2\* changes. (As an example see Figure 5 of Ref. [42] where in the same voxel the post-bolus signal can overshoot or undershoot baseline depending upon the accumulated dose of GBCA.) DSC-MRI signal is thereby affected not only by vascular volume fraction and vessel size, but also by the rate of GBCA extravasation (vascular permeability) and the cell volume fraction, cell size and cell distribution.<sup>28</sup> Signal-time (and  $\Delta R2^*$ -time) curves no longer return to baseline as they do for ideal tracer kinetics, but extend below or above baseline depending on whether T1 or T2\* effects dominate, thereby affecting the accuracy of CBV estimates determined from



the area under the  $\Delta R2^*$ -time curve.<sup>43</sup> The magnitude of this effect depends upon a combination of both DSC-MRI acquisition parameters and contrast agent dosing.<sup>42</sup>

Methods for minimizing DSC-MRI signal contamination from GBCA extravasation include low FA pulse sequences that reduce T1 sensitivity;<sup>44</sup> loading doses or “preload” contrast administration;<sup>5,8,45</sup> and post-processing techniques including model-based leakage correction that can rectify both T1 and T2\* leakage effects.<sup>5,8,45-47</sup> Dual-echo DSC-MRI utilizes two GRE acquisitions with different TEs to estimate change in relaxation rate directly, thereby eliminating T1 contamination effects entirely, but still requires correction for T2\* leakage effects<sup>48</sup> and special pulse sequences that are less widely available.<sup>38,49</sup> No technique has been universally accepted, and much of the debate about best DSC-MRI methodology centers on issues related to minimizing contamination of the DSC-MRI signal due to GBCA extravasation and maximizing CBV accuracy.

Intravascular contrast agents like ferumoxytol eliminate contrast agent leakage effects entirely, and there is compelling evidence that ferumoxytol-based CBV measurements are inherently more accurate and precise than gadolinium-based CBV measurements because complications related to GBCA extravasation are minimized.<sup>50</sup> However, clinical application of ferumoxytol-based DSC-MRI may be limited. FDA-approved as a therapeutic iron supplement, ferumoxytol is less commonly available than GBCA for MRI. GBCAs are widely accepted by radiologists for conventional post-contrast imaging and adding a second contrast agent for DSC-MRI would be logistically challenging. Although conventional contrast-enhanced imaging is feasible with ferumoxytol, it is practically performed 24 hours after agent administration.<sup>51</sup> Furthermore, the standardized BTIP requires post-contrast imaging after one total dose

of GBCA.<sup>30</sup> Finally, gadolinium-based DSC-MRI permits measurement of additional physiological parameters related to GBCA extravasation, such as PSR (percent signal recovery of the signal-time curve compared to baseline), as well as  $K^{trans}$  (volume transfer coefficient of gadolinium from the intravascular to the extravascular, extracellular space). Therefore, we focus on single-GRE GBCA-based DSC-MRI and the selection of four fundamental protocol choices: preload and bolus contrast agent dose, FA, TE, and post-processing leakage correction.

## Preload Contrast Agent Dosing

A “preload” dose of GBCA administered prior to the bolus dose of GBCA given during dynamic imaging can help mitigate T1 contamination. The preload dose partially saturates baseline T1-weighted signal contribution,<sup>5,8,45</sup> thereby diminishing T1-induced increased signal during bolus passage. Evidence supporting preload administration includes data in a C6 rat glioma model, where (at least for high-FA acquisitions) there is no discernable DSC-MRI signal after the first (no preload) injection, and a “usable” DSC-MRI signal for computing CBV with the second injection.<sup>46</sup> A study comparing several different approaches for acquiring and computing rCBV maps in patients demonstrated that without preload, high-grade tumor may mistakenly show no rCBV elevation compared to normal brain, but expected rCBV elevation is found when a preload was used.<sup>42</sup> Preload dosing has varied in the literature, ranging from fractional doses up to a full equivalent dose. In a study using a 60° FA and post-processing leakage correction, Hu et al. found that a full-dose preload of 0.1 mmol/kg and an incubation time of 6 minutes between preload administration and bolus injection optimized the separation of CBVs for

tumor and treatment effect in HGGs with recurrent enhancement after standard chemoradiation.<sup>52</sup>

## Post-Processing Leakage Correction

In practice, DSC-MRI acquisition cannot be decoupled from post-processing, and there is ample evidence that post-processing leakage-correction of DSC-MRI data is necessary for accurate rCBV measurement when the BBB is disrupted.<sup>5,8,45</sup> A pharmacokinetic model-based approach described by Weisskoff et al.<sup>53</sup> was the first published method for correcting T1-based GBCA leakage effects using a linear least-squares fit of the  $\Delta R2^*$ -time curves within the tumor and a reference region in non-enhancing brain to correct the entire  $\Delta R2^*$ -time curve, including first pass.<sup>5,8,45,46</sup> The method was subsequently modified to correct T2\* leakage effects as well,<sup>45,54</sup> and it was empirically determined that the algorithm performed best with the collection of 120 time points, a finding consistent with the assumption of no contrast agent backflux. This leakage correction method is now sometimes referred to as the BSW method (after the authors of the subsequent paper that focused exclusively on the leakage correction algorithm<sup>8</sup>).

Modifications to the BSW approach have since been published, including calculation of the tissue residue function allowing for a voxel-wise correction of the raw DSC-MRI signal that is insensitive to variations in MTT.<sup>46</sup> The ability to determine additional perfusion parameters directly from the residue function has also been demonstrated.<sup>54</sup> Most recently, a “bidirectional” version of the BSW method was developed that accounts for backflux of contrast agent,<sup>47,55</sup> which becomes important with

the collection of >120 time points. While other leakage correction methods like gamma-variate fitting and post-bolus baseline correction have been used, studies suggest that these do not perform as well because they do not correct for leakage effects occurring throughout the DSC bolus.<sup>42,46</sup>

Preload and model-based post-processing leakage correction are synergistic in their improvement of rCBV accuracy,<sup>42</sup> and consensus recommendations for leakage-corrected, single-echo DSC-MRI have been directed towards a technique combining the two methods.<sup>56</sup> For high FA, rCBV using preload plus leakage correction strongly correlates with tumor grade, whereas uncorrected rCBV does not,<sup>8</sup> and in a rat gliosarcoma model, combined preload and post-processing leakage correction yield CBV estimates that converge to gold standard values obtained using MION, an intravascular contrast agent.<sup>57</sup> RCBV measurements using preload and the BSW method agree well with histology in spatially correlated tissue biopsies,<sup>58,59</sup> and the BSW method has been applied in single-institution studies and multi-site clinical trials demonstrating, among other benefits, the utility of rCBV for predicting or detecting early responses to therapy.<sup>20,23,60,61</sup> Nonetheless, there are potentially important improvements to be gained using modified BSW approaches that have yet to be thoroughly evaluated.

Although the BSW method has been implemented by several commercial software vendors, discrepancies in computed rCBV arise in head-to-head comparisons,<sup>62</sup> and caution is recommended for cross-platform comparisons. For instance, significantly different performance was observed when identical DSC-MRI data were processed with two software packages using different implementations of post-processing leakage correction.<sup>62</sup> The best correlation of CBV with histology required preload plus post-

processing leakage correction, providing evidence that leakage correction is important but that technique and implementation matter. Marked inter-site disagreement has also been observed when site-specific software was applied to DSC-MRI data generated by a digital reference object (DRO) using a standardized imaging protocol.<sup>63</sup> Nonetheless, it has been shown that when a single data set is carefully pre-processed eliminating differences in intermediate analysis steps (such as ROI selection and registration), then rCBV values computed by multiple sites using different platforms begin to converge,<sup>64</sup> and a “consensus” threshold is reached for distinguishing low-grade from high-grade gliomas. Therefore, implementation matters, motivating efforts to build consensus regarding post-processing and to establish a benchmark for validating DSC-MRI analysis tools, such as the DRO described below.<sup>65,66</sup>

## **Impact of Flip Angle and TE**

For single-echo DSC-MRI, low to intermediate FA (i.e. 35°–60°) with longer TR (i.e. 1.2–1.7s) and TE (i.e. >20ms) can reduce T1 contamination due to GBCA extravasation.<sup>44</sup> However, some parameter combinations may also reduce the SNR of the computed rCBV maps,<sup>67</sup> and the goal is to minimize leakage effects while maintaining SNR. Accordingly, there are high- and low-FA DSC-MRI strategies with tradeoffs, as summarized in Table 1. Acquisitions using low FA,<sup>44</sup> long TE,<sup>68</sup> and long TR<sup>69</sup> have decreased T1 sensitivity, and less need for preload, but poorer CBV SNR. Higher FA,<sup>8</sup> shorter TE,<sup>70</sup> and shorter TR<sup>67</sup> may require preload to decrease T1 sensitivity, but have higher CBV SNR.

We have direct validation of CBV accuracy using two different acquisition strategies. Stereotactic biopsies co-registered to leakage-corrected CBV maps made with

preload, 60° FA, and post-processing leakage correction have shown excellent correlation of CBV with histologic vascular area and density.<sup>58</sup> Similarly, stereotactic biopsies co-registered to CBV maps made using no preload, a low FA (35°), and no model-based leakage correction also had good correlation of CBV with microvascular expression.<sup>71</sup> The literature is replete with conflicting acquisition strategies such as these.

## **Motivation for Standardization of DSC-MRI Methodology**

The application of DSC-MRI to treatment response assessment of HGGs illustrates the importance of harmonization of DSC-MRI methodology. There has been much investigation of the use of CBV for differentiating true tumor from treatment effects. Relative CBV has putative value for differentiating progressive disease (PD) characterized by enlarged microvessels with high vascular density from treatment effects characterized by inflammatory or steroid-like behavior as in pseudoprogression (PsP) or pseudoresponse, respectively.<sup>72-74</sup>

CBV has been used to distinguish PsP and PD at initial progressive contrast enhancement after chemoradiation but the literature is somewhat conflicting. For instance, Prager et al. studied 68 HGGs at progressive enhancement and found significant difference in median rCBV between PsP and PD, with an optimal threshold of 1.3.<sup>75</sup> Other studies also found mean or median CBV to be predictive, with varying thresholds,<sup>19,76</sup> but others have found mean CBV to be non-predictive or only predictive with qualification. Although Kong et al. found overall significant difference in mean rCBV between PsP and PD, this difference applied to GBMs with unmethylated but not with methylated MGMT.<sup>77</sup> However, a study of HGGs treated with PPX, a powerful radiation sensitizer with a high incidence of PsP often coincident with PD, found no significant

difference in mean rCBV between PsP and PD at initial progressive enhancement.<sup>78</sup> These are just a few examples of varied results in the literature.

## **Variability of DSC-MRI Methodology in the Literature**

Literature results may conflict at least in part because DSC-MRI methodology varies greatly. Patel et al. published a meta-analysis of 17 studies where DSC-MRI was used to differentiate recurrent HGG from treatment-related enhancement.<sup>79</sup> For the subgroup of studies using mean lesion rCBV, they found “relatively good accuracy in individual studies” with high pooled sensitivity (88% [0.81-0.94]) and specificity (88% [0.78-0.95]) for recurrent tumor, but there was a wide range of optimal mean CBV thresholds (0.9–2.15). This variation has been attributed to the wide range of TR, TE, FA, preload dose and post-processing leakage correction used by these studies, as summarized in Figure 1. Variable parameters are also found in subsequent literature. For instance, using spatially correlated histologic tissue samples, TR = 1100-1250ms, TE = 30ms, FA = 70-80°, ½-1 dose preload with full-dose bolus, and post-processing leakage correction (IB Neuro™), Prah et al. found a nRCBV cutoff of 1.13 with 82% sensitivity and 90% specificity.<sup>59</sup> Patel et al. concluded that “because of significant variability in optimal reported thresholds...further investigation and standardization is needed before implementing any particular quantitative PWI strategy across institutions.”

On a similar note, Quarles et al. organized a Quantitative Imaging Network (QIN) DSC-MRI challenge with 12 NCI-QIN centers to explore factors related to CBV consistency.<sup>63</sup> They simulated a 10,000-voxel population-based DRO for each site’s DSC-MRI protocol (19 total protocols),<sup>65</sup> and used corresponding DSC-MRI signal curves

for three evaluations of inter-site CBV consistency: central processing of CBV for site-specific DROs (isolated impact of acquisition protocol); site-specific processing of CBV for standard DRO (isolated impact of post-processing methodology); and site-specific processing of CBV for site-specific DROs (combined impact of acquisition and post-processing). The 3T DSC-MRI acquisition protocol varied considerably for the 12 sites (15 paradigms). Though TR and TE were relatively consistent (possibly reflecting adoption of previously published protocol recommendations<sup>56</sup>), FA and preload dosing varied considerably, with a wide gamut of post-processing methodology, including software, integration limits, and normalization to white matter. When local sites chose both acquisition and post-processing, there was very poor cross-site intra-class correlation for CBV, particularly for simulated blood-brain barrier disruption typical for GBMs, and with large limits of agreement on Bland-Altman analysis. There was better correlation when acquisition or post-processing was standardized, especially post-processing. Overall, this study demonstrates that CBV variability can arise from differences in post-processing as well as image acquisition. This has profound implications for comparing literature CBV values from sites using dissimilar acquisition and post-processing schemes. For clinical trials, although acquisition and post-processing methods are typically standardized, the most accurate and proven approaches should be used for determining the therapeutic effectiveness of a drug, or establishing thresholds for categorical response (e.g., predetermined changes in CBV used to refine RANO criteria).



## **Previous Efforts at Standardization: ASFNR White Paper (2015)**

Efforts at standardization have been made by several organizations including the ASFNR, which published a white paper with the following recommendations: single-echo, GRE pulse sequence; TR = 1.0-1.5s; TE = 40-45ms at 1.5T, 25-35ms at 3T; FA = 60-70°; acquisition duration of at least 120 total time points, including at least 30-50 baseline acquisitions; and  $\frac{1}{4}$ -1 dose preload with full-dose bolus.<sup>56</sup> These recommendations were made prior to the publication of the standardized BTIP,<sup>30</sup> which is gaining clinical acceptance.

## **BTIP Compliance and Implication for Allowable Dosing Schemes**

It is sensible that a standardized DSC-MRI protocol be compatible with BTIP. BTIP mandates that conventional post-contrast T1-weighted imaging be performed after one full dose of GBCA, either split between preload and DSC-MRI bolus before post-contrast imaging, or fully given as preload with variable bolus dose DSC-MRI after post-contrast imaging. This sets constraints on the range of preload and bolus doses that should be considered for inclusion in a universal DSC-MRI protocol. Possible BTIP-compliant DSC-MRI preload and bolus paradigms are illustrated in Figure 2.

## **Selection of Optimal DSC-MRI Parameters: Computational Approach**

Because it is impractical to compare all possible acquisition schemes in vivo, computational approaches have been pursued for determining optimal acquisition parameters.

Using a multi-compartment model-based simulation of DSC-MRI signal derived from convolution theory,<sup>80</sup> the theoretical framework developed by Quarles et al.,<sup>43</sup> and characteristics from 250 randomly chosen tumors, Leu et al. systematically evaluated the effects of various acquisition and post-processing leakage correction strategies, including a range of FA, TE, and TR with BTIP-compliant contrast agent dosing schemes, on the fidelity of CBV estimation in the presence of Gaussian noise.<sup>81</sup> Results of this comprehensive study are summarized in Figure 3. Although no single acquisition scheme was absolutely optimal, several parameter combinations yielded the lowest error in CBV estimation. The best performing acquisition schemes included 60° FA with full-dose preload and full-dose bolus (“1+1” double-dose GBCA), as well as 35° FA without preload. Importantly, high-FA acquisitions with no or fractional preload dosing performed relatively poorly.

Similarly, Semmineh et al. used a validated population-based DRO, derived from 3D tumor tissue microstructures and trained on 23 DSC-MRI glioblastoma datasets including more than 40,000 voxels.<sup>65</sup> They simulated tumor CBV acquired with BTIP-compliant dosing schemes, and a similar range of FA, TE, and TR. Simulated CBV without leakage was the reference standard, and they evaluated concordance correlation coefficient and coefficient of variation as measures of accuracy and precision, respectively. They produced heat maps with similar findings as Leu et al. The best performing schemes used full-dose preload and full-dose bolus at low to intermediate FA, with poor performance for intermediate-high FAs using no or fractional preload, particularly at 1.5 T.<sup>66</sup> Confluent regions of high performance are desirable because these

schemes would presumably be less sensitive to minor parameter variations or to underlying model assumptions or tumor physiology.

Figure 4 summarizes performance of the intermediate 60° FA scheme from the ASFNR white paper versus a high-performing, low FA scheme for TR=1.5s. Full-dose preload with full-dose bolus (“1+1” double-dose GBCA) provides the highest accuracy and precision for both schemes with similar performance at 1.5 and 3T. With intermediate FA, single total dose schemes have poorer performance, especially at 1.5T, with moderate performance for split dose at 3T. Low FA acquisitions give much better performance for single total dose. For single-dose contrast without preload, the ASFNR parameters (i.e., intermediate FA) perform poorly, but low FA maintains excellent performance, even at 1.5T. Non-BTIP compliant preload dosing (e.g., ½ or ¼ dose) with full-dose bolus can give excellent results with low FA and intermediate FA at 3T, and very good results at 1.5T.

Convergence of results from these simulations suggest that even without preload (i.e., “0+1” dosing), a low FA scheme gives very accurate CBV with much less bias compared to intermediate FA, even at 1.5T, and could be an attractive approach requiring less contrast agent (Figure 5A).

With the application of simultaneous multi-slice or multi-band techniques, it is possible to shorten the temporal resolution to sub-second TRs, while maintaining sufficient spatial coverage. DRO-based recommendations for TR, TE, and FA seek the optimal T1 and T2\* sensitivity, and sub-second TRs will increase sensitivity to T1 leakage effects and reduce rCBV fidelity. For example, the DRO analysis for “0+1” dosing and the optimal low FA approach described above (30° FA, 30ms TE) predicts that the

concordance correlation coefficient (CCC), a measure of CBV accuracy, drops to 0.76 and 0.62 for TR=750ms and 500ms, respectively. Even if TE is increased to 50ms, CBV accuracy is lower ( $CCC < 0.9$ ) than that achieved using more conventional TRs (1–1.5s). However, for “1+1” dosing and the optimal low FA scheme, the CCC exceeds 0.95, even for TRs as low as 500ms. These results highlight the importance of parameter consistency and encourage caution when applying acceleration techniques.

### **In vivo Assessment of Low FA, No Preload DSC-MRI**

A recent study was performed to validate in vivo the simulations predicting that single-dose, low-FA DSC-MRI acquisitions without preload (“0+1” dosing) give rCBV estimates practically equivalent to the double-dose, intermediate-FA reference standard using full-dose preload (“1+1” dosing).<sup>82</sup> 84 patients with a contrast-enhancing brain lesion were included in this four-institution study. As shown in Figure 5B, the study demonstrated practical equivalence between the two methods, supporting the idea that this low-dose approach should be considered for consensus protocol recommendation, at least at 3T. The agreement between the two methods was poor if post-processing leakage correction (BSW method) was not also applied. Confirmation of equivalence at 1.5T requires a similar study.

### **Conclusions from Computational Parameter Analyses and In Vivo Comparison Study**

Based on the recent literature, the following conclusions can be drawn regarding DSC-MRI acquisition methodology:

- 1) Of the BTIP-compliant dosing schemes investigated, full-dose preload with full-dose bolus (“1+1” dosing) has superior performance, with the least sensitivity to minor pulse sequence parameter fluctuations and the best combination of accuracy and precision, which is important for clinical trials that aim to minimize sample size. Although both low FA (30°) and intermediate FA (60°) sequences provide a high degree of accuracy in simulations testing the “1+1” dosing scheme, we continue to consider intermediate FA (60°) to be the gold standard for “1+1” dosing, particularly at 3T field strength, given the benefits of higher CNR and lower sensitivity to parameter variations (e.g., TE, TR) compared to low FA (30°) acquisitions.
- 2) When the “1+1” dosing scheme is not desirable (e.g., when prioritizing low GBCA dosage), the no-preload paradigm (“0+1” dosing) with low FA (30°) and an optimally selected and field-strength dependent TE provides an excellent practical alternative to the gold standard and is the recommended alternative method, particularly at 3T for which in vivo validation has been performed. Based on simulation testing of the “0+1” dosing scheme, low FA (30°) acquisitions provide superior accuracy and precision compared to the intermediate FA (60°). This appears to hold true at both 1.5T and 3T field strengths (though has not yet been validated in vivo at 1.5T).
- 3) For both the “1+1” dosing at intermediate FA (60°) and “0+1” dosing at low FA (30°), there is a modest theoretical performance advantage at 3T versus 1.5T.
- 4) For BTIP-compliant fractional dosing (e.g., “ $\frac{1}{2}+\frac{1}{2}$ ” and “ $\frac{1}{4}+\frac{3}{4}$ ” dosing schemes), a low FA (30°) acquisition should be used at all field strengths, given the superior accuracy and precision compared to intermediate FA (60°) acquisitions, with TE = 30-50ms having theoretical advantages, especially at 1.5T. However, these fractional dosing schemes

likely have poorer performance than the “0+1” dosing scheme and the gold-standard “1+1” dosing scheme, due to the theoretical costs of poor CNR for fractional bolus dosing, particularly for perfusion metrics such as cerebral blood flow CBF and MTT.

5) Post-processing leakage correction is always beneficial, even for low FA (30°) acquisitions, and should be utilized in routine practice.

## **Time-point specifications**

### Number of baseline time points

Because the number of baseline acquisitions impacts CBV map SNR, image acquisition should begin at least 30–50 time points before contrast injection via a power injector.<sup>67</sup>

### Number of post-bolus time points

Post-processing leakage-correction algorithms and PSR analysis utilize post-bolus “tail” signal intensities, necessitating acquisition of sufficient post-bolus time points. 120 total time points (for a typical TR of 1.0–1.5s) have been shown by simulation to yield optimal results using the BSW post-processing leakage correction methodology and a 30-50 time point baseline.<sup>66</sup> For longer total acquisitions (e.g., 180 time points), reflux of contrast agent back into blood vessels is more likely to occur, violating assumptions of unidirectional contrast agent efflux.<sup>8</sup> In such cases, bidirectional contrast agent leakage correction schemes are more accurate,<sup>47</sup> with similar accuracy for unidirectional and bidirectional leakage correction when 120 total time points are acquired.<sup>66</sup>

## Compatibility with DCE-MRI

When acquisition of both DCE- and DSC-MRI is desired for a single exam, DCE-MRI is typically performed using the preload dose for DSC-MRI. Preload-based, BTIP-compliant dosing strategies that have been previously evaluated include the “1+1” and “ $\frac{1}{2}+\frac{1}{2}$ ” protocols. Due to the higher CNR of full-dose acquisitions, the “1+1” dosing scheme provides superior DCE- and DSC-parameter accuracy and precision. However, as highlighted in Figure 4, the “ $\frac{1}{2}+\frac{1}{2}$ ” protocol with low FA (30°) provides a reasonable alternative with a modest reduction in accuracy and precision. It is important to note that although the DSC-MRI preload could be used for DCE-MRI, dosage needs to be guided by both DCE-MRI requirements and BTIP compliance, and further investigation is required for determining the fidelity and clinical utility for candidate dosing strategies.

## Summary of Updated Recommendations for DSC-MRI Parameters

In light of the emergence of the BTIP standards,<sup>30</sup> recent computer simulation results,<sup>66,81</sup> and multi-site in vivo validation,<sup>82</sup> our committee is proposing several modifications to the previously published ASFNR recommendations. Because adoption of DSC-MRI is anticipated for multi-site trials, our modified DSC-MRI protocol is BTIP-compliant, imposing constraints on contrast agent preload and bolus selection.

From a theoretical perspective, a full-dose preload, full-dose bolus dosing scheme (“1+1”), using low (30°) or intermediate (60°) FA and field strength-dependent TE (40-50ms at 1.5T, 25-35ms at 3T) provides overall best performance based upon accuracy and precision estimates. In clinical trials or at independent clinical sites where double contrast agent dose is acceptable and highest performance is desired, the double-dose

“1+1”) approach can be used. However, when single-dose GBCA usage is desired or required, we recommend a no-preload, full-dose bolus dosing scheme (“0+1”) using low FA (30°) and field strength-dependent TE (40-50ms at 1.5T, 25-35ms at 3T). For most typical applications and with excellent performance preservation, the “0+1” approach has advantages, including reduced GBCA usage, as well as elimination of potential systematic error introduced by variation in incubation time between preload and bolus administrations. Although the no-preload, low-FA scheme has slightly poorer accuracy and precision than the full-dose preload, full-dose bolus scheme, the “1+1” scheme uses more GBCA, and that downside may more than outweigh the slight gain in performance. Even the fractional dosing schemes (“ $\frac{1}{4}+\frac{3}{4}$ ” and “ $\frac{1}{2}+\frac{1}{2}$ ”), with near equivalent performance using low FA, still have the disadvantage of requiring preload, and potential variation in incubation times can lead to systematic errors. Therefore, the no-preload “0+1” protocol may be most appropriate for routine clinical use.

Post-processing leakage correction is beneficial, even for low FA (30°) acquisitions, and should be utilized in routine practice. The BSW method is an advisable technique for performing post-processing model-based leakage correction and has thus far the most computer simulation and clinical evidence to support its utility. In the absence of universal acceptance of a single software implementation for widespread use, a benchmark may be required for validating independent DSC-MRI post-processing tools, such as the DRO methodology referenced above.

The updated DSC-MRI protocol recommendations are summarized in Table 2. Integrated BTIP and DSC-MRI protocols for the “0+1” and “1+1” dosing schemes are summarized in Supplemental Table 1 and Table 2, respectively.



As a final thought, it is worth noting that although the updated DSC-MRI protocol is motivated by theory, computer simulations, in vivo studies, and clinical trial data related to high-grade gliomas, the principles apply to any contrast-enhancing brain lesion, including metastases and active inflammation or infection. Therefore, we believe that the protocol recommendations herein are generally applicable to routine clinical practice.

## **Funding**

U01 CA176110 (KMS), R01 CA 082500 (KMS), Medical College of Wisconsin Cancer Center (KMS), R01 CA221938 (JLB, CCQ, LSH, KMS) R01 CA213158-01 (CCQ), American Cancer Society (ACS) Research Scholar Grant (RSG-15-003-01-CCE) (Ellingson); American Brain Tumor Association (ABTA) Research Collaborators Grant (ARC1700002)(Ellingson); National Brain Tumor Society (NBTS) Research Grant (Ellingson, Cloughesy); NIH/NCI UCLA Brain Tumor SPORE (1P50CA211015-01A1) (Ellingson, Cloughesy); NIH/NCI 1R21CA223757-01 (Ellingson)

## **Acknowledgments**

We would like to thank additional members of the Jumpstarting Brain Tumor Drug Development Coalition Imaging Standardization Steering Committee including David F. Arons and Ann Kingston from the National Brain Tumor Society (NBTS), Boston, MA, David Sandak and Max Wallace from the Accelerate Brain Cancer Cure (ABC<sup>2</sup>), Washington, D.C., Al Musella from the Musella Foundation, Hewlett, NY, and Chas Haynes from the Collaborative Ependymoma Research Network, Dayton, OH.

## References

1. Rosen BR, Belliveau JW, Vevea JM, Brady TJ. Perfusion imaging with NMR contrast agents. *Magn Reson Med*. 1990; 14(2):249-265.
2. Belliveau JW, Kennedy DN, Jr., McKinstry RC, et al. Functional mapping of the human visual cortex by magnetic resonance imaging. *Science*. 1991; 254(5032):716-719.
3. Aronen HJ, Gazit IE, Louis DN, et al. Cerebral blood volume maps of gliomas: comparison with tumor grade and histologic findings. *Radiology*. 1994; 191(1):41-51.
4. Maeda M, Itoh S, Kimura H, et al. Tumor vascularity in the brain: evaluation with dynamic susceptibility-contrast MR imaging. *Radiology*. 1993; 189(1):233-238.
5. Donahue KM, Krouwer HG, Rand SD, et al. Utility of simultaneously acquired gradient-echo and spin-echo cerebral blood volume and morphology maps in brain tumor patients. *Magn Reson Med*. 2000; 43(6):845-853.
6. Aronen HJ, Pardo FS, Kennedy DN, et al. High microvascular blood volume is associated with high glucose uptake and tumor angiogenesis in human gliomas. *Clin Cancer Res*. 2000; 6(6):2189-2200.
7. Sugahara T, Korogi Y, Kochi M, Ushio Y, Takahashi M. Perfusion-sensitive MR imaging of gliomas: comparison between gradient-echo and spin-echo echo-planar imaging techniques. *AJNR Am J Neuroradiol*. 2001; 22(7):1306-1315.
8. Boxerman JL, Schmainda KM, Weisskoff RM. Relative cerebral blood volume maps corrected for contrast agent extravasation significantly correlate with glioma tumor grade, whereas uncorrected maps do not. *AJNR Am J Neuroradiol*. 2006; 27(4):859-867.

9. Law M, Oh S, Babb JS, et al. Low-grade gliomas: dynamic susceptibility-weighted contrast-enhanced perfusion MR imaging--prediction of patient clinical response. *Radiology*. 2006; 238(2):658-667.
10. Jiang Z, Le Bas JF, Grand S, et al. Prognostic value of perfusion MR imaging in patients with oligodendroglioma: A survival study. *J Neuroradiol*. 2011; 38(1):53-61.
11. Hipp SJ, Steffen-Smith E, Hammoud D, Shih JH, Bent R, Warren KE. Predicting outcome of children with diffuse intrinsic pontine gliomas using multiparametric imaging. *Neuro-oncology*. 2011; 13(8):904-909.
12. Bonekamp D, Deike K, Wiestler B, et al. Association of overall survival in patients with newly diagnosed glioblastoma with contrast-enhanced perfusion MRI: Comparison of intraindividually matched T1 - and T2 (\*) -based bolus techniques. *Journal of magnetic resonance imaging : JMRI*. 2015; 42(1):87-96.
13. Jabehdar Maralani P, Melhem ER, Wang S, et al. Association of dynamic susceptibility contrast enhanced MR Perfusion parameters with prognosis in elderly patients with glioblastomas. *Eur Radiol*. 2015; 25(9):2738-2744.
14. Barajas RF, Jr., Chang JS, Segal MR, et al. Differentiation of recurrent glioblastoma multiforme from radiation necrosis after external beam radiation therapy with dynamic susceptibility-weighted contrast-enhanced perfusion MR imaging. *Radiology*. 2009; 253(2):486-496.
15. Hu LS, Baxter LC, Smith KA, et al. Relative cerebral blood volume values to differentiate high-grade glioma recurrence from posttreatment radiation effect: direct correlation between image-guided tissue histopathology and localized dynamic

susceptibility-weighted contrast-enhanced perfusion MR imaging measurements. *AJNR Am J Neuroradiol*. 2009; 30(3):552-558.

16. Gasparetto EL, Pawlak MA, Patel SH, et al. Posttreatment recurrence of malignant brain neoplasm: accuracy of relative cerebral blood volume fraction in discriminating low from high malignant histologic volume fraction. *Radiology*. 2009; 250(3):887-896.
17. Kim HS, Goh MJ, Kim N, Choi CG, Kim SJ, Kim JH. Which combination of MR imaging modalities is best for predicting recurrent glioblastoma? Study of diagnostic accuracy and reproducibility. *Radiology*. 2014; 273(3):831-843.
18. Hu LS, Eschbacher JM, Heiserman JE, et al. Reevaluating the imaging definition of tumor progression: perfusion MRI quantifies recurrent glioblastoma tumor fraction, pseudoprogression, and radiation necrosis to predict survival. *Neuro-oncology*. 2012; 14(7):919-930.
19. Young RJ, Gupta A, Shah AD, et al. MRI perfusion in determining pseudoprogression in patients with glioblastoma. *Clin Imaging*. 2013; 37(1):41-49.
20. Schmainda KM, Prah M, Connelly J, et al. Dynamic-susceptibility contrast agent MRI measures of relative cerebral blood volume predict response to bevacizumab in recurrent high-grade glioma. *Neuro-oncology*. 2014; 16(6):880-888.
21. Leu K, Enzmann DR, Woodworth DC, et al. Hypervascular tumor volume estimated by comparison to a large-scale cerebral blood volume radiographic atlas predicts survival in recurrent glioblastoma treated with bevacizumab. *Cancer Imaging*. 2014; 14:31.

22. Aquino D, Di Stefano AL, Scotti A, et al. Parametric response maps of perfusion MRI may identify recurrent glioblastomas responsive to bevacizumab and irinotecan. *PLoS One*. 2014; 9(3):e90535.
23. Schmainda KM, Zhang Z, Prah M, et al. Dynamic Susceptibility Contrast MRI Measures of Relative Cerebral Blood Volume as a Prognostic Marker for Overall Survival in Recurrent Glioblastoma: Results from the ACRIN 6677/RTOG 0625 Multi-Center Trial. *Neuro-oncology*. 2015; 17(8):1148-1156.
24. Kickingeder P, Wiestler B, Burth S, et al. Relative cerebral blood volume is a potential predictive imaging biomarker of bevacizumab efficacy in recurrent glioblastoma. *Neuro-oncology*. 2015; 17(8):1139-1147.
25. Harris RJ, Cloughesy TF, Hardy AJ, et al. MRI perfusion measurements calculated using advanced deconvolution techniques predict survival in recurrent glioblastoma treated with bevacizumab. *Journal of neuro-oncology*. 2015; 122(3):497-505.
26. Geer CP, Simonds J, Anvery A, et al. Does MR perfusion imaging impact management decisions for patients with brain tumors? A prospective study. *AJNR Am J Neuroradiol*. 2012; 33(3):556-562.
27. Willats L, Calamante F. The 39 steps: evading error and deciphering the secrets for accurate dynamic susceptibility contrast MRI. *NMR Biomed*. 2013; 26(8):913-931.
28. Semmineh NB, Xu J, Skinner JT, et al. Assessing tumor cytoarchitecture using multiecho DSC-MRI derived measures of the transverse relaxivity at tracer equilibrium (TRATE). *Magn Reson Med*. 2015; 74(3):772-784.

29. Stokes AM, Skinner JT, Yankeelov T, Quarles CC. Assessment of a simplified spin and gradient echo (sSAGE) approach for human brain tumor perfusion imaging. *Magn Reson Imaging*. 2016; 34(9):1248-1255.
30. Ellingson BM, Bendszus M, Boxerman J, et al. Consensus recommendations for a standardized Brain Tumor Imaging Protocol in clinical trials. *Neuro-oncology*. 2015; 17(9):1188-1198.
31. Meier P, Zierler KL. On the theory of the indicator-dilution method for measurement of blood flow and volume. *J Appl Physiol*. 1954; 6(12):731-744.
32. Villringer A, Rosen BR, Belliveau JW, et al. Dynamic imaging with lanthanide chelates in normal brain: contrast due to magnetic susceptibility effects. *Magn Reson Med*. 1988; 6(2):164-174.
33. Rempp KA, Brix G, Wenz F, Becker CR, Guckel F, Lorenz WJ. Quantification of regional cerebral blood flow and volume with dynamic susceptibility contrast-enhanced MR imaging. *Radiology*. 1994; 193(3):637-641.
34. Bedekar D, Jensen T, Schmainda KM. Standardization of relative cerebral blood volume (rCBV) image maps for ease of both inter- and inpatient comparisons. *Magn Reson Med*. 2010; 64(3):907-913.
35. Ellingson BM, Zaw T, Cloughesy TF, et al. Comparison between intensity normalization techniques for dynamic susceptibility contrast (DSC)-MRI estimates of cerebral blood volume (CBV) in human gliomas. *Journal of magnetic resonance imaging : JMRI*. 2012; 35(6):1472-1477.

36. Boxerman JL, Hamberg LM, Rosen BR, Weisskoff RM. MR contrast due to intravascular magnetic susceptibility perturbations. *Magn Reson Med*. 1995; 34(4):555-566.
37. Fisel CR, Ackerman JL, Buxton RB, et al. MR contrast due to microscopically heterogeneous magnetic susceptibility: numerical simulations and applications to cerebral physiology. *Magn Reson Med*. 1991; 17(2):336-347.
38. Schmiedeskamp H, Straka M, Newbould RD, et al. Combined spin- and gradient-echo perfusion-weighted imaging. *Magn Reson Med*. 2012; 68(1):30-40.
39. Zama A, Tamura M, Inoue HK. Three-dimensional observations on microvascular growth in rat glioma using a vascular casting method. *J Cancer Res Clin Oncol*. 1991; 117(5):396-402.
40. Badruddoja MA, Krouwer HG, Rand SD, Rebro KJ, Pathak AP, Schmainda KM. Antiangiogenic effects of dexamethasone in 9L gliosarcoma assessed by MRI cerebral blood volume maps. *Neuro-oncology*. 2003; 5(4):235-243.
41. Weisskoff RM, Zuo CS, Boxerman JL, Rosen BR. Microscopic susceptibility variation and transverse relaxation: theory and experiment. *Magn Reson Med*. 1994; 31(6):601-610.
42. Paulson ES, Schmainda KM. Comparison of dynamic susceptibility-weighted contrast-enhanced MR methods: recommendations for measuring relative cerebral blood volume in brain tumors. *Radiology*. 2008; 249(2):601-613.
43. Quarles CC, Gochberg DF, Gore JC, Yankeelov TE. A theoretical framework to model DSC-MRI data acquired in the presence of contrast agent extravasation. *Phys Med Biol*. 2009; 54(19):5749-5766.

44. Cha S, Knopp EA, Johnson G, Wetzel SG, Litt AW, Zagzag D. Intracranial mass lesions: dynamic contrast-enhanced susceptibility-weighted echo-planar perfusion MR imaging. *Radiology*. 2002; 223(1):11-29.
45. Schmainda KM, Rand SD, Joseph AM, et al. Characterization of a first-pass gradient-echo spin-echo method to predict brain tumor grade and angiogenesis. *AJNR Am J Neuroradiol*. 2004; 25(9):1524-1532.
46. Quarles CC, Ward BD, Schmainda KM. Improving the reliability of obtaining tumor hemodynamic parameters in the presence of contrast agent extravasation. *Magn Reson Med*. 2005; 53(6):1307-1316.
47. Leu K, Boxerman JL, Lai A, et al. Bidirectional Contrast agent leakage correction of dynamic susceptibility contrast (DSC)-MRI improves cerebral blood volume estimation and survival prediction in recurrent glioblastoma treated with bevacizumab. *Journal of magnetic resonance imaging : JMRI*. 2016; 44(5):1229-1237.
48. Paulson ES, Prah DE, Schmainda KM. Spiral Perfusion Imaging With Consecutive Echoes (SPICE) for the Simultaneous Mapping of DSC- and DCE-MRI Parameters in Brain Tumor Patients: Theory and Initial Feasibility. *Tomography*. 2016; 2(4):295-307.
49. Vonken EP, van Osch MJ, Bakker CJ, Viergever MA. Simultaneous quantitative cerebral perfusion and Gd-DTPA extravasation measurement with dual-echo dynamic susceptibility contrast MRI. *Magn Reson Med*. 2000; 43(6):820-827.
50. Gahramanov S, Muldoon LL, Li X, Neuwelt EA. Improved perfusion MR imaging assessment of intracerebral tumor blood volume and antiangiogenic therapy efficacy in a rat model with ferumoxytol. *Radiology*. 2011; 261(3):796-804.



51. Horvath A, Varallyay CG, Schwartz D, et al. Quantitative comparison of delayed ferumoxytol T1 enhancement with immediate gadoteridol enhancement in high grade gliomas. *Magn Reson Med*. 2018; 80(1):224-230.
52. Hu LS, Baxter LC, Pinnaduwa DS, et al. Optimized preload leakage-correction methods to improve the diagnostic accuracy of dynamic susceptibility-weighted contrast-enhanced perfusion MR imaging in posttreatment gliomas. *AJNR Am J Neuroradiol*. 2010; 31(1):40-48.
53. Weisskoff RM, Boxerman JL, Sorensen AG, Kulke SM, Campbell TA, Rosen BR. Simultaneous blood volume and permeability mapping using a single Gd-based contrast injection. Paper presented at: Society of Magnetic Resonance in Medicine, 2nd Annual Meeting 1994; San Francisco, CA.
54. Bjornerud A, Sorensen AG, Mouridsen K, Emblem KE. T1- and T2\*-dominant extravasation correction in DSC-MRI: part I--theoretical considerations and implications for assessment of tumor hemodynamic properties. *J Cereb Blood Flow Metab*. 2011; 31(10):2041-2053.
55. Leu K, Boxerman JL, Cloughesy TF, et al. Improved Leakage Correction for Single-Echo Dynamic Susceptibility Contrast Perfusion MRI Estimates of Relative Cerebral Blood Volume in High-Grade Gliomas by Accounting for Bidirectional Contrast Agent Exchange. *AJNR Am J Neuroradiol*. 2016; 37(8):1440-1446.
56. Welker K, Boxerman J, Kalnin A, et al. ASFNR recommendations for clinical performance of MR dynamic susceptibility contrast perfusion imaging of the brain. *AJNR Am J Neuroradiol*. 2015; 36(6):E41-51.

57. Boxerman JL, Prah DE, Paulson ES, Machan JT, Bedekar D, Schmainda KM. The Role of preload and leakage correction in gadolinium-based cerebral blood volume estimation determined by comparison with MION as a criterion standard. *AJNR Am J Neuroradiol*. 2012; 33(6):1081-1087.
58. Hu LS, Eschbacher JM, Dueck AC, et al. Correlations between perfusion MR imaging cerebral blood volume, microvessel quantification, and clinical outcome using stereotactic analysis in recurrent high-grade glioma. *AJNR Am J Neuroradiol*. 2012; 33(1):69-76.
59. Prah MA, Al-Gizawiy MM, Mueller WM, et al. Spatial discrimination of glioblastoma and treatment effect with histologically-validated perfusion and diffusion magnetic resonance imaging metrics. *Journal of neuro-oncology*. 2018; 136(1):13-21.
60. Prah MA, Stufflebeam SM, Paulson ES, et al. Repeatability of Standardized and Normalized Relative CBV in Patients with Newly Diagnosed Glioblastoma. *AJNR Am J Neuroradiol*. 2015; 36(9):1654-1661.
61. Gerstner ER, Zhang Z, Fink JR, et al. ACRIN 6684: Assessment of Tumor Hypoxia in Newly Diagnosed Glioblastoma Using 18F-FMISO PET and MRI. *Clin Cancer Res*. 2016; 22(20):5079-5086.
62. Hu LS, Kelm Z, Korfiatis P, et al. Impact of Software Modeling on the Accuracy of Perfusion MRI in Glioma. *AJNR Am J Neuroradiol*. 2015; 36(12):2242-2249.
63. Bell LC, Semmineh N, An H, et al. Evaluating Multisite rCBV Consistency from DSC-MRI Imaging Protocols and Postprocessing Software Across the NCI Quantitative Imaging Network Sites Using a Digital Reference Object (DRO). *Tomography*. 2019; 5(1):110-117.

64. Schmainda KM, Prah MA, Rand SD, et al. Multisite Concordance of DSC-MRI Analysis for Brain Tumors: Results of a National Cancer Institute Quantitative Imaging Network Collaborative Project. *AJNR Am J Neuroradiol*. 2018; 39(6):1008-1016.
65. Semmineh NB, Stokes AM, Bell LC, Boxerman JL, Quarles CC. A Population-Based Digital Reference Object (DRO) for Optimizing Dynamic Susceptibility Contrast (DSC)-MRI Methods for Clinical Trials. *Tomography*. 2017; 3(1):41-49.
66. Semmineh NB, Bell LC, Stokes AM, Hu LS, Boxerman JL, Quarles CC. Optimization of Acquisition and Analysis Methods for Clinical Dynamic Susceptibility Contrast (DSC) MRI Using a Population-based Digital Reference Object. *AJNR Am J Neuroradiol*. 2018; 39(11):1981-1988.
67. Boxerman JL, Rosen BR, Weisskoff RM. Signal-to-noise analysis of cerebral blood volume maps from dynamic NMR imaging studies. *Journal of magnetic resonance imaging : JMRI*. 1997; 7(3):528-537.
68. Thilmann O, Larsson EM, Bjorkman-Burtscher IM, Stahlberg F, Wirestam R. Effects of echo time variation on perfusion assessment using dynamic susceptibility contrast MR imaging at 3 tesla. *Magn Reson Imaging*. 2004; 22(7):929-935.
69. Knutsson L, Stahlberg F, Wirestam R. Aspects on the accuracy of cerebral perfusion parameters obtained by dynamic susceptibility contrast MRI: a simulation study. *Magn Reson Imaging*. 2004; 22(6):789-798.
70. Smith MR, Lu H, Frayne R. Signal-to-noise ratio effects in quantitative cerebral perfusion using dynamic susceptibility contrast agents. *Magn Reson Med*. 2003; 49(1):122-128.

71. Barajas RF, Jr., Hodgson JG, Chang JS, et al. Glioblastoma multiforme regional genetic and cellular expression patterns: influence on anatomic and physiologic MR imaging. *Radiology*. 2010; 254(2):564-576.
72. Das S, Marsden PA. Angiogenesis in glioblastoma. *The New England journal of medicine*. 2013; 369(16):1561-1563.
73. Brandsma D, van den Bent MJ. Pseudoprogression and pseudoresponse in the treatment of gliomas. *Current opinion in neurology*. 2009; 22(6):633-638.
74. Wen PY, Macdonald DR, Reardon DA, et al. Updated response assessment criteria for high-grade gliomas: response assessment in neuro-oncology working group. *J Clin Oncol*. 2010; 28(11):1963-1972.
75. Prager AJ, Martinez N, Beal K, Omuro A, Zhang Z, Young RJ. Diffusion and perfusion MRI to differentiate treatment-related changes including pseudoprogression from recurrent tumors in high-grade gliomas with histopathologic evidence. *AJNR Am J Neuroradiol*. 2015; 36(5):877-885.
76. Mangla R, Singh G, Ziegelitz D, et al. Changes in relative cerebral blood volume 1 month after radiation-temozolomide therapy can help predict overall survival in patients with glioblastoma. *Radiology*. 2010; 256(2):575-584.
77. Kong DS, Kim ST, Kim EH, et al. Diagnostic dilemma of pseudoprogression in the treatment of newly diagnosed glioblastomas: the role of assessing relative cerebral blood flow volume and oxygen-6-methylguanine-DNA methyltransferase promoter methylation status. *AJNR Am J Neuroradiol*. 2011; 32(2):382-387.

- 78.** Boxerman JL, Ellingson BM, Jeyapalan S, et al. Longitudinal DSC-MRI for Distinguishing Tumor Recurrence From Pseudoprogession in Patients With a High-grade Glioma. *Am J Clin Oncol*. 2017; 40(3):228-234.
- 79.** Patel P, Baradaran H, Delgado D, et al. MR perfusion-weighted imaging in the evaluation of high-grade gliomas after treatment: a systematic review and meta-analysis. *Neuro-oncology*. 2017; 19(1):118-127.
- 80.** Ostergaard L, Weisskoff RM, Chesler DA, Gyldensted C, Rosen BR. High resolution measurement of cerebral blood flow using intravascular tracer bolus passages. Part I: Mathematical approach and statistical analysis. *Magn Reson Med*. 1996; 36(5):715-725.
- 81.** Leu K, Boxerman JL, Ellingson BM. Effects of MRI Protocol Parameters, Preload Injection Dose, Fractionation Strategies, and Leakage Correction Algorithms on the Fidelity of Dynamic-Susceptibility Contrast MRI Estimates of Relative Cerebral Blood Volume in Gliomas. *AJNR Am J Neuroradiol*. 2017; 38(3):478-484.
- 82.** Schmainda KM, Prah MA, Hu LS, et al. Moving Toward a Consensus DSC-MRI Protocol: Validation of a Low-Flip Angle Single-Dose Option as a Reference Standard for Brain Tumors. *AJNR Am J Neuroradiol*. 2019.

## Figure Captions

### Figure 1.

DSC-MRI methodology in the literature varies greatly, as seen in the subgroup meta-analysis by Patel et al. of studies using mean lesion rCBV for recurrent high-grade tumor vs. treatment effect. These studies used a wide range of DSC-MRI parameters including TE, FA, preload dose and post-processing leakage correction (PPLC). (Adapted from Ref. [79].)

### Figure 2.

Possible BTIP-compliant DSC-MRI preload + bolus dose paradigms. Either a single total dose must be split between preload and DSC-MRI before post-GBCA imaging, or a full dose preload must be given with DSC-MRI after post-contrast imaging.

### Figure 3.

Computational approach for determining optimal BTIP-compliant DSC-MRI parameters using simulated DSC-MRI signal with GBCA leakage: heat maps of CBV error versus theoretical CBV without leakage for different combinations of acquisition parameters. Schemes with particularly high fidelity at 3T include 60° FA with full-dose preload and bolus (asterisk with dashed box) and low FA without preload (asterisk with solid box). (Adapted from Ref. [81].)

### Figure 4.

Computational approach for determining optimal BTIP-compliant DSC-MRI parameters using a digital reference object matched to glioblastoma training data: performance comparison for intermediate and low flip angle schemes. For double-dose contrast with

full-dose preload, both schemes have excellent accuracy and precision at 1.5T and 3T. For single-dose contrast without preload, intermediate FA performs poorly but low FA maintains excellent performance, even at 1.5T. For each dosing scheme, low FA had equal or better performance than intermediate FA. CCC = Concordance correlation coefficient (accuracy); CV = coefficient of variation (precision). (Adapted from Ref. [66].)

**Figure 5.**

- A) DRO-based simulations demonstrate that even without preload, low FA (30°) acquisitions give very accurate CBV (along the line of unity) with much less bias compared to intermediate FA (60°) acquisitions, even at 1.5T. (Adapted from Ref. [66].)
- B) Excellent CBV agreement has been observed in vivo at 3T for “0+1” and “1+1” dosing schemes, according to Lin’s concordance correlation (CCC).

Table 1: Summary of CBV SNR and T1 sensitivity tradeoffs for DSC-MRI acquisition strategies

Acquisition Parameters

Parameter	CBV SNR	T1 sensitivity	Reference
Flip angle			
Low	Decrease	<b>Decrease</b>	Cha et al. Radiology 2002 <sup>44</sup>
High	<b>Increase</b>	Increase	Boxerman et al. AJNR 2006 <sup>8</sup>
TE			
Long	Decrease	<b>Decrease</b>	Thilmann Et al. MRI 2004 <sup>68</sup>
Short	<b>Increase</b>	Increase	Smith et al. MRM 2003 <sup>70</sup>
TR			
Long	Decrease	<b>Decrease</b>	Knutsson et al. MRI 2004 <sup>69</sup>
Short	<b>Increase</b>	Increase	Boxerman et al. JMRI 1997 <sup>67</sup>

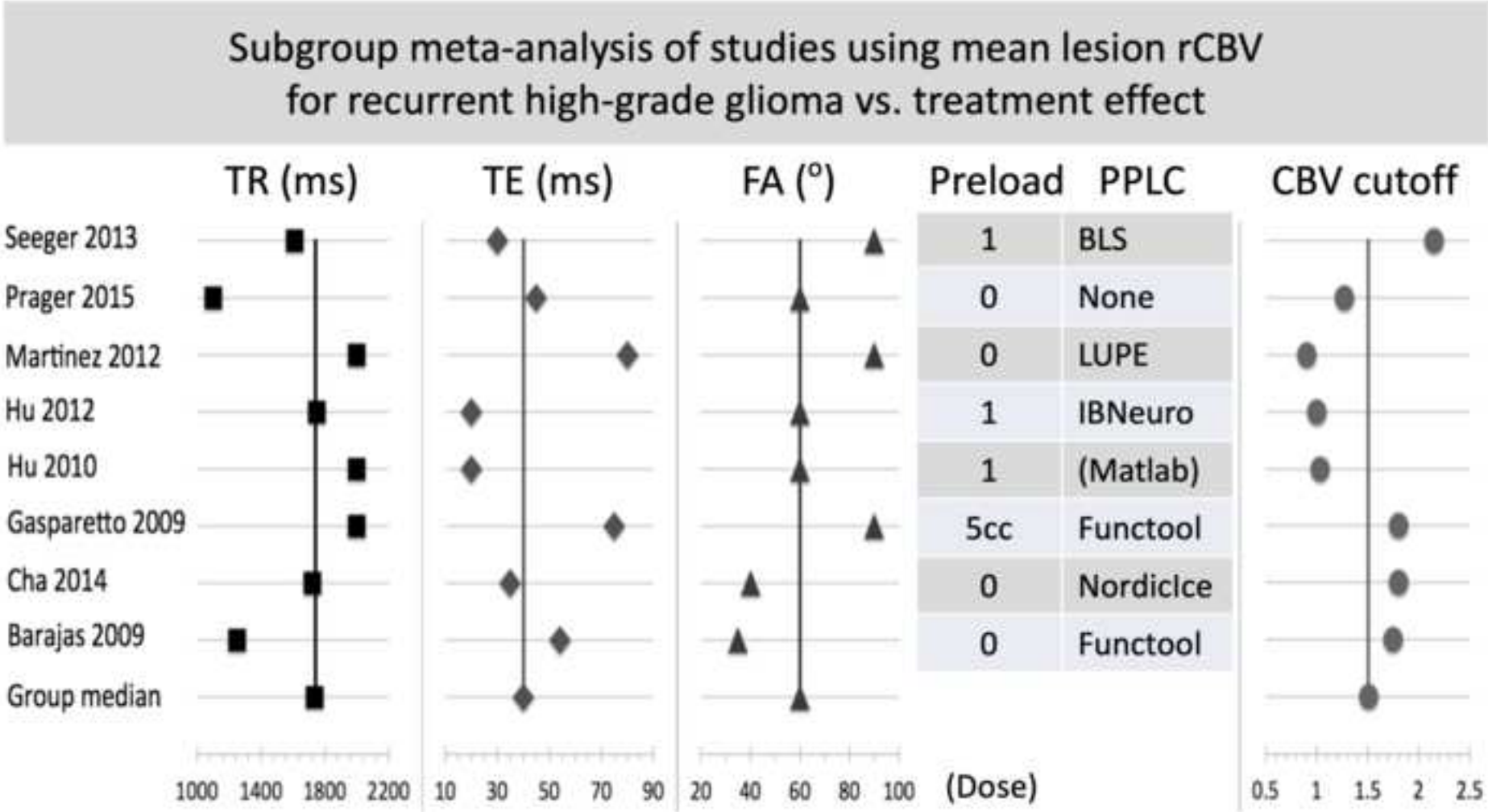
Preload contrast agent administration

Pros	Cons	Reference
Decreased T1 sensitivity	Extra contrast agent	Donahue et al. MRM 2000 <sup>5</sup>
	Variable incubation time	Hu et al. AJNR 2010 <sup>52</sup>



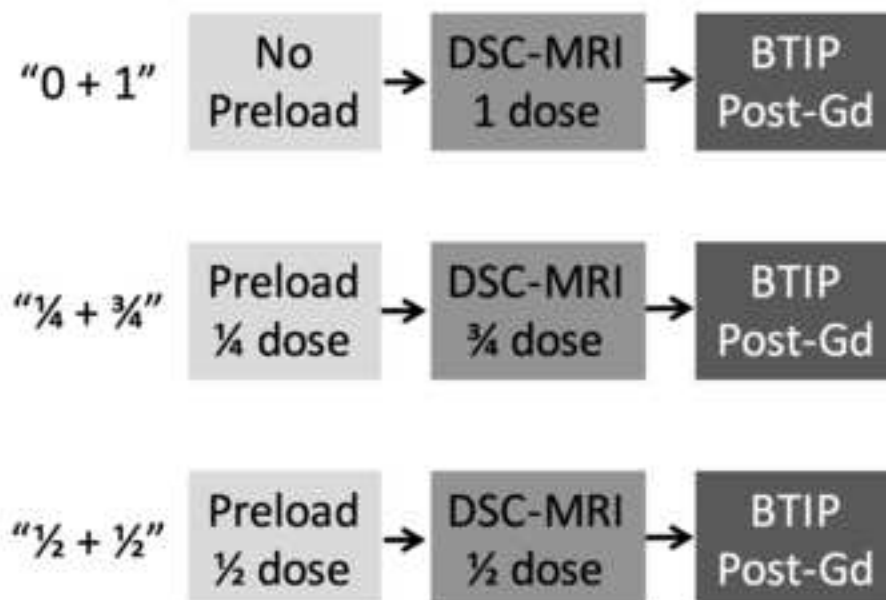
**Table 2: Summary of protocol recommendations for BTIP-compliant DSC-MRI**

Parameter	3T Recommendations (Range)	1.5T Recommendations (Range)
Pulse sequence	GRE-EPI	
Plane	Axial (Oblique Axial)	
Mode	2D	
Dosing protocol (preload + bolus)	“1 + 1”: Optimal performance (Preload → T1w+C → DSC bolus injection) “0 + 1”: Optimal for single total dose (DSC bolus injection → T1w+C)	
Repetition Time (TR) (msec)	1000-1500	
Echo Time (TE) (msec)	30 (25 – 35) for 30° FA 30 (20 – 35) for 60° FA	45 (40 – 50)
Flip Angle (FA) (deg)	60 (60-65) or 30 (30-35) (“1 + 1” dosing) 30 (30-35) (“0 + 1” dosing)	
Total time points	≥ 120	
Baseline time points	50 (30 – 50)	
Field of view (mm)	(220 – 240)	
Acquisition matrix	128 x 128 (96-128 x 96-128)	≥ 96 x 96 (96-128 x 96-128)
Slice thickness (mm)	3 (3-5), as needed for tumor coverage	4 (4-5), as needed for tumor coverage
Slice gap (mm)	0 (0 – 1), as needed for tumor coverage	
Parallel imaging (GRAPPA/SENSE/CAIPI)	≤ 2x	
Post-processing leakage correction	Model-based BSW ( <i>Unidirectional</i> , or <i>Bidirectional</i> for > 120 time points)	

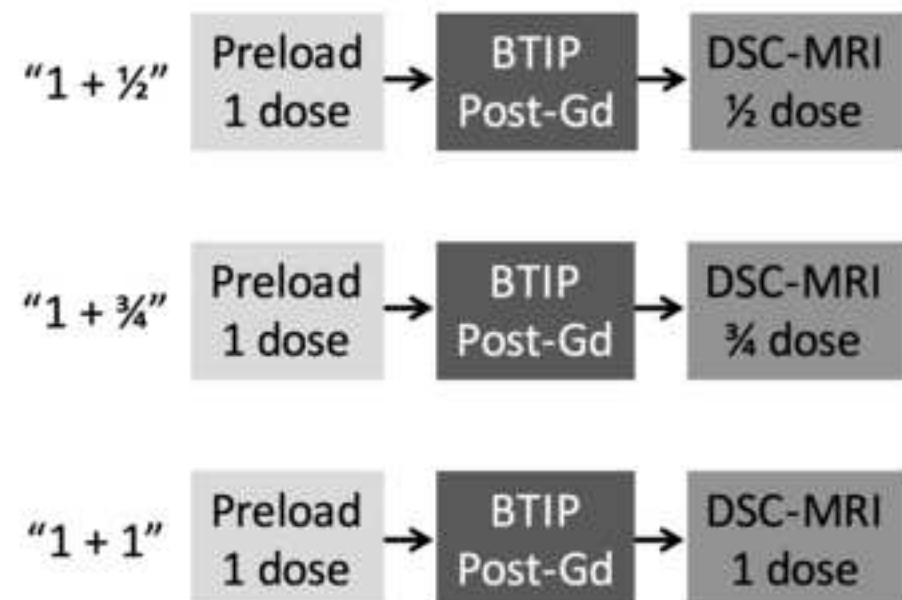


## Possible BTIP-Compliant DSC-MRI Preload/Bolus Paradigms

### Single total dose

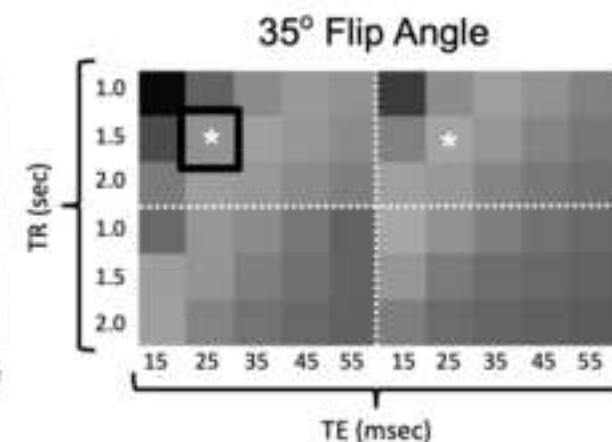
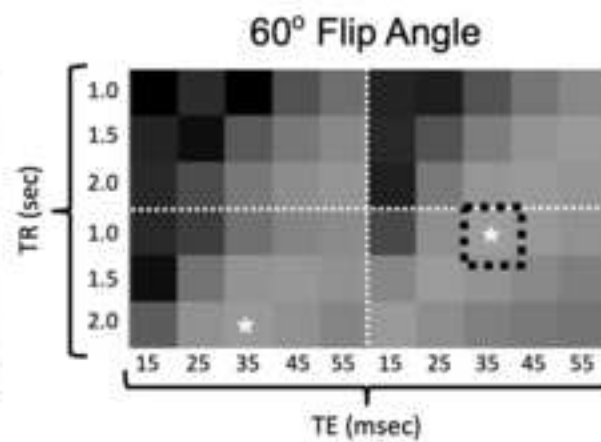
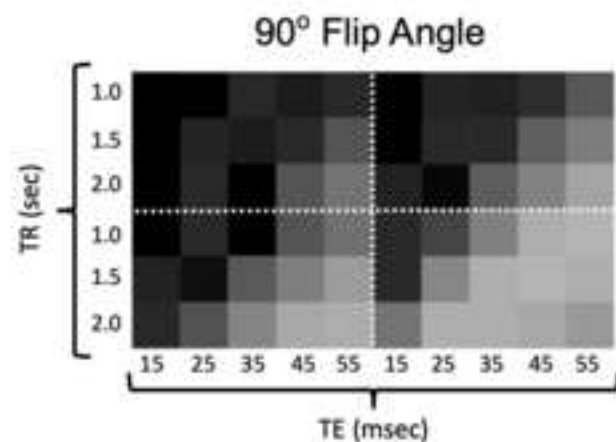
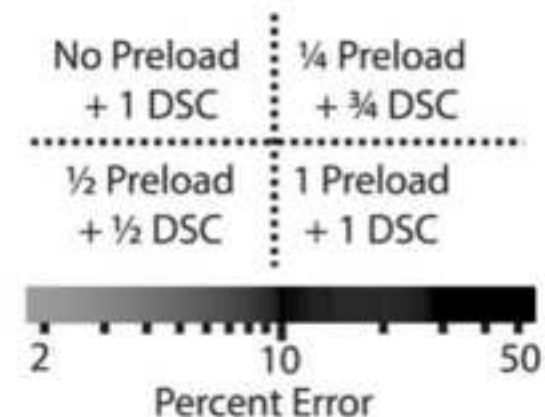


### 1<sup>+</sup> – Double total dose



## Optimal BTIP-compliant DSC-MRI parameters: Multi-compartment model-based simulation

Flip angle (°)	TE (ms)	TR (s)	Dose (Pre + bolus)
35	35	1.5	0 + 1
35	25	1.5	$\frac{1}{4}$ + $\frac{3}{4}$
60	35	2.0	$\frac{1}{2}$ + $\frac{1}{2}$
60	35	1.0	1 + 1



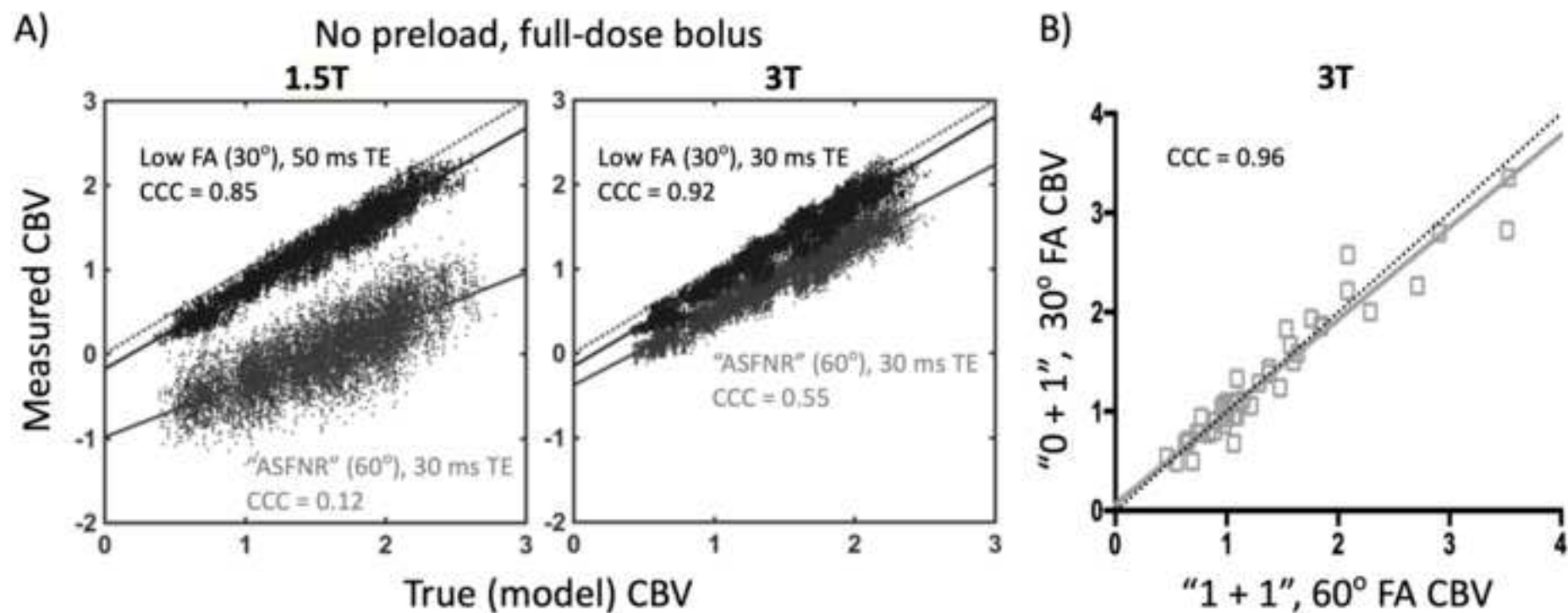
## Optimal BTIP-compliant DSC-MRI parameters: Comparison of low FA and intermediate FA acquisitions

Intermediate flip angle  
(ASFNR white paper)  
FA=60°, TE=30ms, TR=1.5s

Low flip angle  
1.5T: FA=30°, TE=50ms, TR=1.5s  
3.0T: FA=30°, TE=30ms, TR=1.5s

	Dosing (PLD + Bolus)	Intermediate flip angle (ASFNR white paper) FA=60°, TE=30ms, TR=1.5s				Low flip angle 1.5T: FA=30°, TE=50ms, TR=1.5s 3.0T: FA=30°, TE=30ms, TR=1.5s			
		1.5 T		3 T		1.5 T		3 T	
		CCC	CV (%)	CCC	CV (%)	CCC	CV (%)	CCC	CV (%)
BTIP-compliant	1 + 1	0.92	7.4	0.97	6.6	0.96	7.4	0.98	6.8
	½ + ½	0.44	16.3	0.76	9.2	0.89	10.8	0.90	8.7
	¼ + ¼	0.38	18.2	0.74	8.8	0.91	9.0	0.94	7.8
	0 + 1	0.12	41.4	0.55	12.4	0.85	9.3	0.92	8.2
Non-BTIP	¼ + 1	0.77	8.2	0.93	6.8	0.95	7.7	0.97	7.0
	½ + 1	0.87	7.8	0.96	6.8	0.95	7.5	0.97	6.8

## Comparison of low FA and intermediate FA acquisitions: Simulation and in vivo



Supplemental TABLE 1: “0+1” 1.5T & 3T MRI PROTOCOL

	3D T1w Pre <sup>b</sup>	Ax 2D FLAIR <sup>f</sup>	Ax 2D DWI	Ax 2D T2w <sup>e</sup>	DSC-MRI <sup>a</sup>	3D T1w Post <sup>b</sup>
Sequence	IR-GRE <sup>d</sup>	TSE <sup>c</sup>	EPI	TSE <sup>c</sup>	GRE EPI	IR-GRE <sup>d</sup>
Plane	Sagittal/Axial	Axial	Axial	Axial	Axial	Sagittal/Axial
Mode	3D	2D	2D	2D	2D	3D
TR [ms]	2100 <sup>k</sup>	>6000	>5000	>2500	1000-1500	2100 <sup>k</sup>
TE [ms]	Min	100-140	Min	80-120	3T: 30 (25-35) 1.5T: 45 (40-50)	Min
TI [ms]	1100 <sup>j</sup>	2000-2500 <sup>g</sup>				1100 <sup>j</sup>
Flip Angle [°]	10-15	90/≥160	90/180	90/≥160	30 (30-35)	10-15
Frequency	256	≥256	≥128	256	128 (96-128)	256
Phase	256	≥256	≥128	256	128 (96-128)	256
NEX	≥1	≥1	≥1	≥1	1	≥1
FOV [mm]	256	240	240	240	220-240	256
Slice Thickness [mm]	1	≤4 <sup>h</sup>	≤4 <sup>h</sup>	4 <sup>h</sup>	3-5 <sup>i</sup>	1
Gap/Spacing [mm]	0	0	0	0	0 <sup>i</sup>	0
Diffusion Options <sup>l</sup>			<i>b</i> = 0, 500, 1000 s/mm <sup>2</sup> ≥3 directions			
Perfusion Timepoints					50 (30-50) baseline, ≥120 total	
Parallel Imaging	Up to 2x	Up to 2x	Up to 2x	Up to 2x	Up to 2x	Up to 2x
Scan Time (Approx) [Benchmarked on 3T Skyra]	5-10 min [5:49 for 1mm isotropic]	4-8 min [3:22 for 2D FLAIR]	2-4 min [1:22 for 3 direction DWI and 3 b-values]	4-8 min	2-3 min	5-10 min [5:49 for 1mm isotropic]



- <sup>a</sup> 0.1 mmol/kg dose injection with a Gadolinium chelated contrast agent. Use of a power injector at an injection rate of 3-5cc/sec. Maximize slice coverage to include the entire lesion as well as normal brain to the skull vertex. The posterior fossa can be excluded from coverage if there are not enough slices to cover the entire brain.
- <sup>b</sup> Post-contrast 3D T1-weighted images should be collected with equivalent parameters to pre-contrast 3D T1-weighted images
- <sup>c</sup> TSE = turbo spin echo (Siemens & Philips) is equivalent to FSE (fast spin echo; GE, Hitachi, Toshiba)
- <sup>d</sup> IR-GRE = inversion-recovery gradient-recalled echo sequence is equivalent to MPRAGE = magnetization prepared rapid gradient-echo (Siemens & Hitachi) and the inversion recovery spoiled gradient-echo (IR-SPGR or Fast SPGR with inversion activated or BRAVO; GE), 3D turbo field echo (TFE; Philips), or 3D fast field echo (3D Fast FE; Toshiba). A 3D acquisition without inversion preparation will result in different contrast compared with MPRAGE or another IR-prepped 3D T1-weighted sequences and therefore should be avoided.
- <sup>e</sup> Dual echo PD/T2 TSE is optional for possible quantification of tissue T2. For this sequence, PD is recommended to have a TE < 25ms.
- <sup>f</sup> 3D FLAIR is an optional alternative to 2D FLAIR, with sequence parameters as follows per EORTC guidelines: 3D TSE/FSE acquisition; TE=90-140ms; TR=6000-10000ms; TI=2000-2500ms (chosen based on vendor recommendations for optimized protocol and field strength); GRAPPA≤2; Fat Saturation; Slice thickness ≤ 1.5mm; Orientation Sagittal or Axial; FOV ≤ 250 mm x 250 mm; Matrix ≥ 244x244.
- <sup>g</sup> Choice of TI should be chosen based on the magnetic field strength of the system (e.g. TI ≈ 2000ms for 1.5T and TI ≈ 2500ms for 3T).
- <sup>h</sup> In order to ensure comparable SNR older 1.5T MR systems can use contiguous (no interslice gap) images with 5mm slice thickness or increase NEX for slice thickness ≤4mm.
- <sup>i</sup> Slice thickness and inter-slice gap can be adjusted as needed for tumor coverage.
- <sup>j</sup> For Siemens and Hitachi scanners. GE, Philips, and Toshiba scanners should use a TI = 400-450ms for similar contrast.
- <sup>k</sup> For Siemens and Hitachi scanners. GE, Philips, and Toshiba scanners should use a TR = 5-15ms for similar contrast.
- <sup>l</sup> Older model MR scanners that are not capable of >2 *b*-values should use *b* = 0 and 1000 s/mm<sup>2</sup>.

#### Acronyms:

Ax = Axial; ADC = apparent diffusion coefficient. FLAIR = fluid attenuated inversion recovery; DWI = diffusion-weighted imaging; 3D = three dimensional; TSE = turbo spin echo; EPI = echo planar imaging; SS-EPI = single-shot echo planar imaging; GRE EPI = gradient echo echo planar imaging; MPRAGE = magnetization prepared rapid gradient-echo; A/P = anterior to posterior; R/L = right to left; NEX = number of excitations or averages; FOV = field of view; TE = echo time; TR = repetition time; TI = inversion time; PD = proton density; DSC = dynamic susceptibility contrast; IR-GRE = inversion-recovery gradient-recalled echo



Supplemental TABLE 2: “1+1” 1.5T & 3T MRI PROTOCOL

	3D T1w Pre <sup>b</sup>	Ax 2D FLAIR <sup>f</sup>	Ax 2D DWI	Preload Contrast Injection <sup>a</sup>	Ax 2D T2w <sup>e</sup>	3D T1w Post <sup>b</sup>	DSC-MRI <sup>m</sup>
Sequence	IR-GRE <sup>d</sup>	TSE <sup>c</sup>	EPI		TSE <sup>c</sup>	IR-GRE <sup>d</sup>	GRE-EPI
Plane	Sagittal/Axial	Axial	Axial		Axial	Axial/Sagittal	Axial
Mode	3D	2D	2D		2D	3D	2D
TR [ms]	2100 <sup>k</sup>	>6000	>5000		>2500	2100 <sup>k</sup>	1000-1500
TE [ms]	Min	100-140	Min		80-120	Min	3T: 30 (20-35) 1.5T: 45 (40-50)
TI [ms]	1100 <sup>i</sup>	2000-2500 <sup>g</sup>				1100 <sup>i</sup>	
Flip Angle [°]	10-15	90/≥160	90/180		90/≥160	10-15	60 (60-65)
Frequency	256	≥256	≥128		256	256	128 (96-128)
Phase	256	≥256	≥128		256	256	128 (96-128)
NEX	≥1	≥1	≥1		≥1	≥1	1
FOV [mm]	256	240	240		240	256	220-240
Slice Thickness [mm]	1	≤4 <sup>h</sup>	≤4 <sup>h</sup>		≤4 <sup>h</sup>	1	3-5i
Gap/Spacing [mm]	0	0	0		0	0	0
Diffusion Options <sup>l</sup>			<i>b</i> = 0, 500, 1000 s/mm <sup>2</sup> ≥3 directions				
Perfusion Timepoints							50 (30-50) baseline, 120 total
Parallel Imaging	Up to 2x	Up to 2x	Up to 2x		Up to 2x	Up to 2x	Up to 2x
Scan Time (Approx) [Benchmarked on 3T Skyra]	5-10 min [5:49 for 1mm isotropic]	4-8 min [3:22 for 2D FLAIR]	2-4 min [1:22 for 3 direction DWI and 3 b-values]		4-8 min	5-10 min [5:49 for 1mm isotropic]	2-3 min

<sup>a</sup> 0.10 mmol/kg (1 dose) preload should be injected 1-2 minutes prior to DSC-MRI acquisition.

<sup>b</sup> Post-contrast 3D T1-weighted images should be collected with equivalent parameters to pre-contrast 3D T1-weighted images

<sup>c</sup> TSE = turbo spin echo (Siemens & Philips) is equivalent to FSE (fast spin echo; GE, Hitachi, Toshiba)

<sup>d</sup> IR-GRE = inversion-recovery gradient-recalled echo sequence is equivalent to MPRAGE = magnetization prepared rapid gradient-echo (Siemens & Hitachi) and the inversion recovery spoiled gradient-echo (IR-SPGR or Fast SPGR with inversion activated or BRAVO; GE), 3D turbo field echo (TFE; Philips), or 3D fast field echo (3D Fast FE; Toshiba). A 3D acquisition without inversion preparation will result in different contrast compared with MPRAGE or another IR-prepped 3D T1-weighted sequences and therefore should be avoided.

<sup>e</sup> Dual echo PD/T2 TSE is optional for possible quantification of tissue T2. For this sequence, PD is recommended to have a TE < 25ms.

<sup>f</sup> 3D FLAIR is an optional alternative to 2D FLAIR, with sequence parameters as follows per EORTC guidelines: 3D TSE/FSE acquisition; TE=90-140ms; TR=6000-10000ms; TI=2000-2500ms (chosen based on vendor recommendations for optimized protocol and field strength); GRAPPA≤2; Fat Saturation; Slice thickness ≤ 1.5mm; Orientation Sagittal or Axial; FOV ≤ 250 mm x 250 mm; Matrix ≥ 244x244.

<sup>g</sup> Choice of TI should be chosen based on the magnetic field strength of the system (e.g. TI ≈ 2000ms for 1.5T and TI ≈ 2500ms for 3T).

<sup>h</sup> In order to ensure comparable SNR older 1.5T MR systems can use contiguous (no interslice gap) images with 5mm slice thickness or increase NEX for slice thickness ≤4mm.

<sup>i</sup> Slice thickness and inter-slice gap can be adjusted as needed for tumor coverage.

<sup>j</sup> For Siemens and Hitachi scanners. GE, Philips, and Toshiba scanners should use a TI = 400-450ms for similar contrast.

<sup>k</sup> For Siemens and Hitachi scanners. GE, Philips, and Toshiba scanners should use a TR = 5-15ms for similar contrast.

<sup>l</sup> Older model MR scanners that are not capable of >2 *b*-values should use *b* = 0 and 1000 s/mm<sup>2</sup>.

<sup>m</sup> 0.1 mmol/kg (1 dose) injection with a Gadolinium chelated contrast agent. Use of a power injector at an injection rate of 3-5cc/sec. Maximize slice coverage to include the entire lesion as well as normal brain to the skull vertex. The posterior fossa can be excluded from coverage if there are not enough slices to cover the entire brain.

#### Acronyms:

Ax = Axial; ADC = apparent diffusion coefficient. FLAIR = fluid attenuated inversion recovery; DWI = diffusion-weighted imaging; 3D = three dimensional; TSE = turbo spin echo; EPI = echo planar imaging; SS-EPI = single-shot echo planar imaging; GRE EPI = gradient echo echo planar imaging; MPRAGE = magnetization prepared rapid gradient-echo; A/P = anterior to posterior; R/L = right to left; NEX = number of excitations or averages; FOV = field of view; TE = echo time; TR = repetition time; TI = inversion time; PD = proton density; DSC = dynamic susceptibility contrast; IR-GRE = inversion-recovery gradient-recalled echo